LETTERS
https://doi.org/10.1038/s41477-022-01134-w

nature plants

Check for updates

A conserved module regulates receptor kinase signalling in immunity and development

Thomas A. DeFalco[1,2,7], Pauline Anne[3,7], Sean R. James[4,7], Andrew C. Willoughby[4], Florian Schwanke[1], Oliver Johanndrees[1,6], Yasmine Genolet[3], Paul Derbyshire[2], Qian Wang[3], Surbhi Rana[3], Anne-Marie Pullen[4], Frank L. H. Menke[2], Cyril Zipfel[1,2]✉, Christian S. Hardtke[3]✉ and Zachary L. Nimchuk[4,5]✉

Ligand recognition by cell-surface receptors underlies development and immunity in both animals and plants. Modulating receptor signalling is critical for appropriate cellular responses but the mechanisms ensuring this are poorly understood. Here, we show that signalling by plant receptors for pathogen-associated molecular patterns (PAMPs) in immunity and CLAVATA3/EMBRYO SURROUNDING REGION-RELATED peptides (CLEp) in development uses a similar regulatory module. In the absence of ligand, signalling is dampened through association with specific type-2C protein phosphatases. Upon activation, PAMP and CLEp receptors phosphorylate divergent cytosolic kinases, which, in turn, phosphorylate the phosphatases, thereby promoting receptor signalling. Our work reveals a regulatory circuit shared between immune and developmental receptor signalling, which may have broader important implications for plant receptor kinase-mediated signalling in general.

Receptor kinases (RKs) perceive the immediate cellular environment[1]. Leucine-rich repeat (LRR)-RKs represent the largest group of RKs in plants, with >220 members in the model plant *Arabidopsis thaliana* (hereafter, *Arabidopsis*)[2,3]. LRR-RKs perceive a wide variety of ligands to regulate diverse aspects of growth, development, reproduction and stress responses[1]. How specificity in LRR-RK signalling is achieved is poorly understood, owing to a lack of known signalling mechanisms and intermediates for many LRR-RK pathways. Several of the best-studied LRR-RKs to date function as cell-surface immune receptors, which perceive pathogen-associated molecular patterns (PAMPs) or endogenous damage-associated molecular patterns (DAMPs) or phytocytokines to regulate immunity. In particular, the *Arabidopsis* LRR-RKs FLAGELLIN SENSING 2 (FLS2) and ELONGATION FACTOR TU RECEPTOR (EFR) perceive the bacterial PAMPs flagellin (or its peptide epitope flg22) and elongation factor-Tu (or its peptide epitope elf18), respectively, to regulate pattern-triggered immunity (PTI)[4–6].

An emerging common theme in RK signalling is the involvement of receptor-like cytoplasmic kinases (RLCKs). RLCKs are homologous to RKs but lack an extracellular domain and are thought to act in downstream RK signalling[7]. Members of the large RLCK-VII/PBS1-LIKE (PBL) family in particular have emerged as key components of LRR-RK-mediated signalling, such as the close homologues BOTRYTIS-INDUCED KINASE1 (BIK1) and PBL1, which act downstream of several immune-related RKs, including FLS2 and EFR[8–11] and are thus key executors of PTI[12].

Modulation of receptor signalling is critical to prevent inappropriate activation and previous work has implicated several protein phosphatases in LRR-RK-mediated immune signalling[13–16], including the *Arabidopsis* specific type-2C protein phosphatases (PP2Cs) POLTERGEIST-LIKE 4 and 5 (PLL4 and PLL5) and their rice homologue XB15, which were identified as negative regulators of EFR- and XA21-mediated PTI, respectively[14,15]. Accordingly, *pll4 pll5* mutants exhibited accelerated kinetics of reactive oxygen species (ROS) production in response to the PAMPs elf18 and flg22 as well as to the DAMP peptide AtPep1 (Fig. 1a,b), indicating that like BIK1 (ref. [17]), PLL4 and PLL5 are common components of PTI signalling downstream of multiple LRR-RKs.

When expressed as a maltose-binding protein (MBP)-fusion protein, wild type (WT) but not catalytically dead PLL4 (PLL4*, D280N/D573N) directly dephosphorylated the autophosphorylated cytosolic domain of EFR (EFR-CD) in vitro (Fig. 1c). Interestingly, truncation of the non-catalytic N terminus rendered PLL4 inactive in this assay, in contrast to previous work with the related phosphatase POLTERGEIST (POL)[18], suggesting an important role for this N-terminal region.

It was previously shown that elf18 perception induced dissociation of PLL4 and PLL5 from EFR in planta[14]; however, the mechanisms mediating such dissociation remain unknown. We observed a similar flg22-induced dissociation of PLL4 and PLL5 from FLS2 in planta using transient expression in *Nicotiana benthamiana* (Extended Data Fig. 1), in keeping with our observation that these phosphatases also regulate FLS2 signalling (Fig. 1a,b). To understand how PLL4 and PLL5 are themselves regulated, we interrogated public databases[19,20] for phosphosites within these proteins. Several clustered, conserved sites were identified in the N terminus of PLL4 and PLL5 that conformed to a previously identified [S/T]-X-X-L motif (Fig. 1d and Extended Data Fig. 2), which is targeted by BIK1 and PBL1 in other substrates[10,21].

BIK1 specifically trans-phosphorylated full-length MBP-PLL4* (catalytically dead PLL4 was used as a substrate to preclude any effect of phosphatase activity) in vitro, confirming that PLL4 is a bona fide BIK1 substrate (Fig. 1e). We then performed liquid

[1]Institute of Plant and Microbial Biology and Zürich-Basel Plant Science Center, University of Zürich, Zurich, Switzerland. [2]The Sainsbury Laboratory, University of East Anglia, Norwich Research Park, Norwich, UK. [3]Department of Plant Molecular Biology, University of Lausanne, Lausanne, Switzerland. [4]Department of Biology, University of North Carolina at Chapel Hill, Chapel Hill, NC, USA. [5]Curriculum in Genetics and Molecular Biology, University of North Carolina at Chapel Hill, Chapel Hill, NC, USA. [6]Present address: Max Planck Institute for Plant Breeding Research, Cologne, Germany. [7]These authors contributed equally: Thomas A. DeFalco, Pauline Anne, Sean R. James. ✉e-mail: cyril.zipfel@botinst.uzh.ch; christian.hardtke@unil.ch; zackn@email.unc.edu

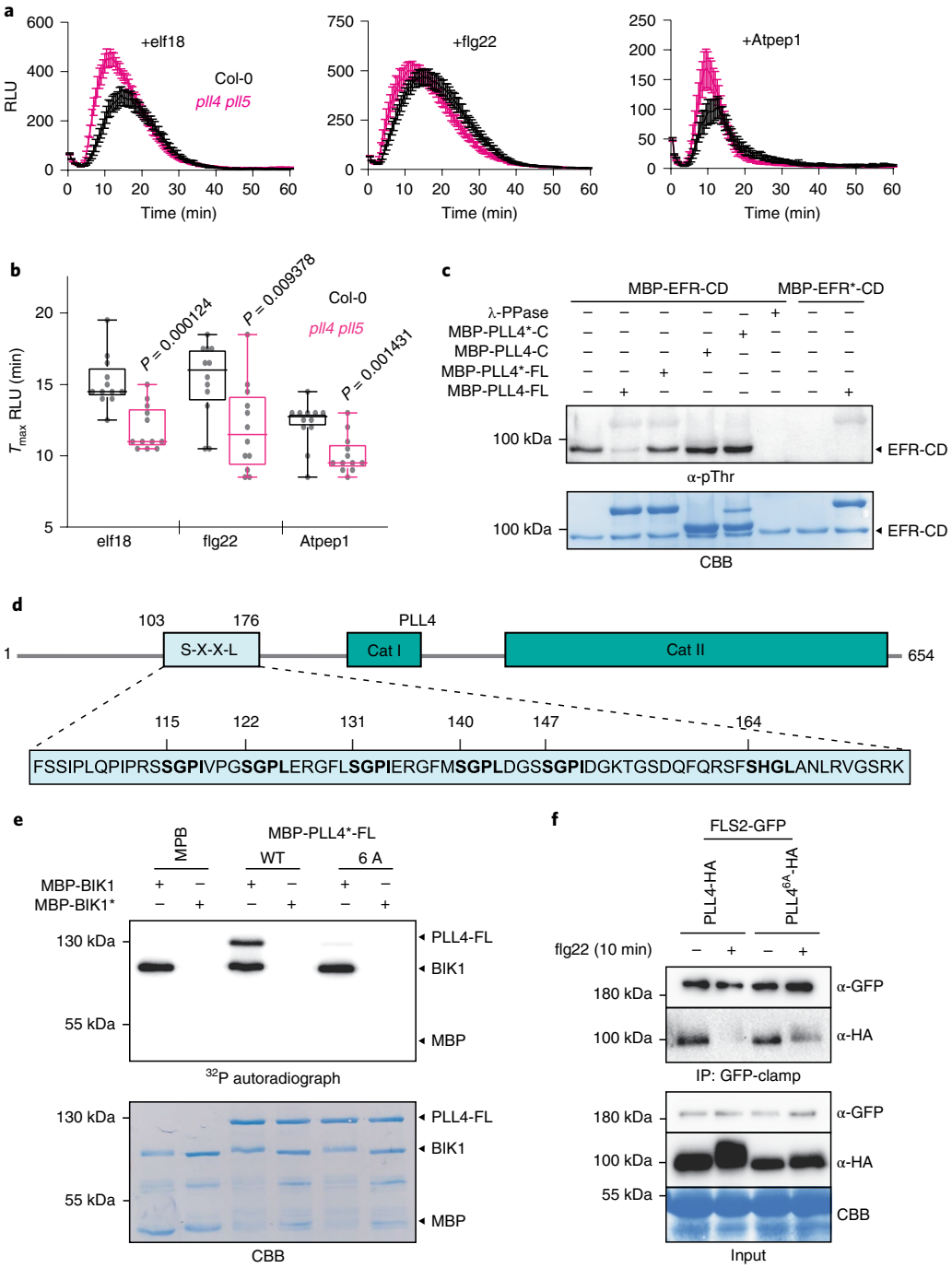

Fig. 1 | A BIK1-PLL regulatory circuit controls PTI activation. a,**b**, PLL4 and PLL5 regulate ROS burst induction by elf18 (100 nM), flg22 (100 nM) or AtPep1 (1 μM) treatments on 4.5-week-old *Arabidopsis* leaf discs in Col-0 WT and *pll4 pll5* backgrounds. **a**, Values correspond to the mean of $n = 12$ independent leaf discs (± s.e.) and are expressed in relative light units (RLU). **b**, Histograms represent the time to maximum RLU (T_{max} RLU) of $n = 12$ independent biological replicates (± s.d.). *P* values from two-tailed *t*-tests are indicated. Box plots show 25th to 75th percentile range with a line at the median and whiskers from minimum to maximum values. **c**, PLL4 can dephosphorylate EFR in vitro. In vitro phosphatase assay incubating equal amounts of MBP-tagged full-length (FL) or C-terminal (C) WT (PLL4) or inactive PLL4 (PLL4*) with autophosphorylated cytosolic domain of MBP-tagged EFR (EFR-CD). The phosphorylation of MBP-EFR-CD WT or kinase dead (EFR*) was detected by anti-phosphothreonine western blot. **d**, Schematic representation of PLL4 domains and details of the S-X-X-L domain of PLL4 and PLL5 homologues. Bold amino acids indicate the S-X-X-L motifs targeted for mutagenesis in PLL4^{6A} or PLL4^{6D}; numbers correspond to the amino acid positions within the protein. **e**, BIK1 phosphorylates the PLL4 N terminus in a site-specific manner. Autoradiogram of in vitro kinase assay using WT BIK1 or inactive (BIK1*) BIK1 with FL WT or phosphovariant (PLL4^{6A}) MBP-PLL4*. **f**, In planta flg22-triggered PLL4 dissociation from FLS2 is regulated by phosphorylation. CoIP assay of transiently expressed FLS2-GFP and HA-tagged PLL4 or PLL4^{6A} in *N. benthamiana* leaves with or without 100 nM flg22 treatment for 10 min. CBB, Coomassie brilliant blue. All experiments were performed at least three times with similar results.

chromatography (LC)–mass spectrometry (MS)/MS to identify BIK1-mediated phosphosites on MBP-PLL4*. Most identified sites corresponded to the tandem consensus motifs found within this N-terminal S-X-X-L domain (Extended Data Fig. 3a), with L substituted to I in some cases (Fig. 1d), which agrees with previous studies showing that BIK1 targets highly specific motifs within substrate proteins, both in vitro and in vivo[10,11,21]. To confirm the specificity of BIK1 phosphorylation, we mutated six putative motif-conforming sites within the PLL4 N terminus (Fig. 1d) to phospho-dead variants ($PLL4^{6A}$). In assays using either full-length PLL4 or the PLL4 N terminus (PLL4-N), BIK1-mediated trans-phosphorylation of PLL4 was abolished with $PLL4^{6A}$ (Fig. 1e and Extended Data Fig. 3b), demonstrating that BIK1 specifically phosphorylates these clustered, tandem sites in the PLL4 N terminus, at least in vitro.

To understand how PLL4 phosphorylation regulates its function, we compared phospho-dead (PLL^{6A}) or phospho-mimetic ($PLL4^{6D}$) mutant variants. Because we were unable to obtain stable transgenic *pll4 pll5* lines expressing native promoter-driven PLL4 variants, possibly due to the autoimmunity of *pll4 pll5* plants, we examined the in planta function of PLL4 phosphorylation using heterologous expression in *N. benthamiana*. Treatment with flg22 induced a phosphorylation-dependent shift in the mobility of PLL4 in *N. benthamiana*, which was not observed with $PLL4^{6A}$ (Fig. 1f and Extended Data Fig. 3c), suggesting that these N-terminal sites become phosphorylated upon ligand perception. The flg22-induced dissociation of $PLL4^{6A}$ from FLS2 was partially compromised (Fig. 1f), whereas MBP-$PLL4^{6D}$ displayed impaired direct interaction with EFR-CD in vitro (Extended Data Fig. 3d). Consistent with a negative role for phosphorylation in PLL4 function, the kinetics of ROS production upon elicitor treatment were dampened by $PLL4^{6A}$, while $PLL4^{6D}$ had no effect (Extended Data Fig. 3e), whereas the plasma membrane association was unaffected in either PLL4 variant (Extended Data Fig. 3f). Together, these data indicate a negative regulatory role for N-terminal phosphorylation on PLL4 function and support a model wherein N-terminal phosphorylation promotes the dissociation of PLL4 from the immune RK complex.

Aside from immunity, many LRR-RKs regulate diverse growth and developmental processes; however, the downstream signalling components of these pathways are often still poorly characterized. LRR-RKs of the CLAVATA 1 (CLV1) and BARELY ANY MERISTEM (BAM1–3) clade perceive endogenous CLAVATA3/EMBRYO SURROUNDING REGION-RELATED (CLE) family peptides[22,23]. CLE peptides (CLEp) are broadly conserved across land plants[24] and regulate important aspects of plant development including stem cell niche maintenance and root development[25,26]. Despite the biological importance of CLEp signalling, the molecular components of such pathways are mostly unknown.

In an unbiased forward genetic screen to identify new components of the CLEp pathway[27], two independently isolated mutants were recovered on the basis of their dominant insensitivity to CLE26p[28]; and both mutants carried an L135F amino acid change in the RLCK-VII subfamily member PBL34. This dominant negative allele (*pbl34-2*) not only conferred insensitivity to CLE26p but also to other root-active CLE peptides (Fig. 2a), indicating that PBL34 is required for CLEp signalling. Matching these observations, a *PBL34* null allele (*pbl34-3*) displayed quantitative insensitivity to the same range of root-active CLE peptides (Fig. 2a). The activation of BIK1 by RK-mediated phosphorylation is well-characterized[12] and, consistent with a role downstream of CLEp perception, PBL34 and the cytosolic domain of the CLEp receptor BAM3 (BAM3-CD) were able to directly phosphorylate each other in vitro (Fig. 2b).

L135 of PBL34 is highly conserved across the RLCK-VII/PBL family (Extended Data Fig. 4). To understand the dominant negative effect of the *pbl34-2* allele, we expressed recombinant PBL34 bearing the causative L135F mutation and tested its kinase activity in vitro. Both auto- and trans-phosphorylation activities of $PBL34^{L135F}$ were severely reduced compared to WT (Fig. 2c), indicating that kinase activity is essential for PBL34 function in CLEp signalling.

PBL34 belongs to the RLCK-VII-5 subfamily together with PBL35 and PBL36 (ref. [29]). Comparison of single and double mutants in these *PBL* genes revealed that each contributes quantitatively to CLEp sensitivity in root elongation assays (Extended Data Fig. 5a,b). A loss-of-function mutant of all three RLCK-VII-5 subfamily members (*rlck-vii-5*) led to strongly increased CLEp insensitivity (Fig. 2d and Extended Data Fig. 5a-c), comparable or superior to the *pbl34-2* mutant (Extended Data Fig. 5d). A screen of all *rlck-vii* subfamily polymutants[29] revealed that this CLEp insensitivity was unique to *rlck-vii-5*, indicating that RLCK-VII-5 subfamily PBLs are specifically required for CLEp signalling (Fig. 2d). Notably, the same PBLs were recently similarly implicated in CLEp signalling[30]. In agreement with roles in CLEp signalling, transcriptional reporters indicated that all three *RLCK-VII-5* subfamily members are expressed in the root (Fig. 2e).

Expression of a PBL34-CITRINE (PBL34-CIT) fusion protein under control of the *PBL34* promoter complemented CLEp responsiveness in the loss-of-function *pbl34-3* single mutant (Extended Data Fig. 5e,f) as well as the *rlck-vii-5* polymutant (Extended Data Fig. 5g,h), corroborating the predominant role of PBL34 within the clade. PBL34-CIT displayed plasma membrane association (Fig. 2f,g) and was broadly expressed in both the root and shoot apical meristems (Fig. 2f and Extended Data Fig. 5i), consistent with a role in CLEp signalling immediately downstream of CLEp receptors. The CLEp-insensitive *pbl34-2* mutant had no effect on immune-related ROS production (Extended Data Fig. 5k), while the

Fig. 2 | The RLCK-VII-5 subfamily is required for CLEp signalling. a, The *pbl34-2* dominant negative allele is less sensitive to exogenous CLEp than the *pbl34-3* loss-of-function allele. Seven-day-old seedlings were grown on media with 50 nM of indicated CLE peptides. NT, not treated. Letters indicate significant differences within the treatments (ANOVA followed by Tukey test). $n = 11$–50 independent biological replicates. Box plots show 25th to 75th percentile range with a line at the median and whiskers from minimum to maximum values. **b**, BAM3 and PBL34 transphosphorylate each other in vitro. Autoradiogram of in vitro kinase assay using MBP-tagged WT PBL34 or inactive PBL34 (PBL34*) and GST-tagged WT cytosolic domain (CD) of BAM3 (BAM3-CD) or inactive CD of BAM3 (BAM3*-CD). **c**, The L135F mutation disrupts auto- and trans-phosphorylation activity of PBL34. Autoradiogram of in vitro kinase assay incubating equal amounts of GST-tagged BAM3 with MBP-tagged WT PBL34 or mutant forms of PBL34 ($PBL34^{D275A}$ or $PBL34^{L135F}$). Kinase assays in **b** and **c** were performed twice with similar results. **d**, CLV3p responses specifically require the *RLCK-VII-5* subfamily. Seven-day-old seedlings were grown on media with CLV3p as indicated. NT, not treated. Letters indicate significant differences within the treatments (ANOVA followed by Tukey test, two-sided). $n = 26$–46. Box plots show 25th to 75th percentile range with a line at the median and whiskers from minimum to maximum values. **e**, *RLCK-VII-5* members are expressed in the root with partially overlapping patterns. Confocal microscopy pictures of 6-day-old seedlings carrying *PBL34::3xNLS-VENUS*, *PBL35::3xNLS-VENUS* and *PBL36::3xNLS-VENUS* constructs, respectively, in Col-0 background. Yellow channel, 3xNLS-VENUS; cyan, propidium iodide cell wall staining. **f**,**g**, *PBL34* is expressed in the root, accumulates in the protophloem and localizes to the cytosol and the plasma membrane. **f**, Confocal microscopy images of 5-day-old seedlings expressing PBL34-CIT fusion protein under control of the *PBL34* promoter in the *rlck-vii-5* triple mutant. PBL34-CIT is detected by anti-GFP immunostaining; yellow channel, CIT; cyan, Calcofluor white cell wall staining. **g**, Intensity trace of a protophloem cell file showing plasma membrane localization of PBL34-CIT signal.

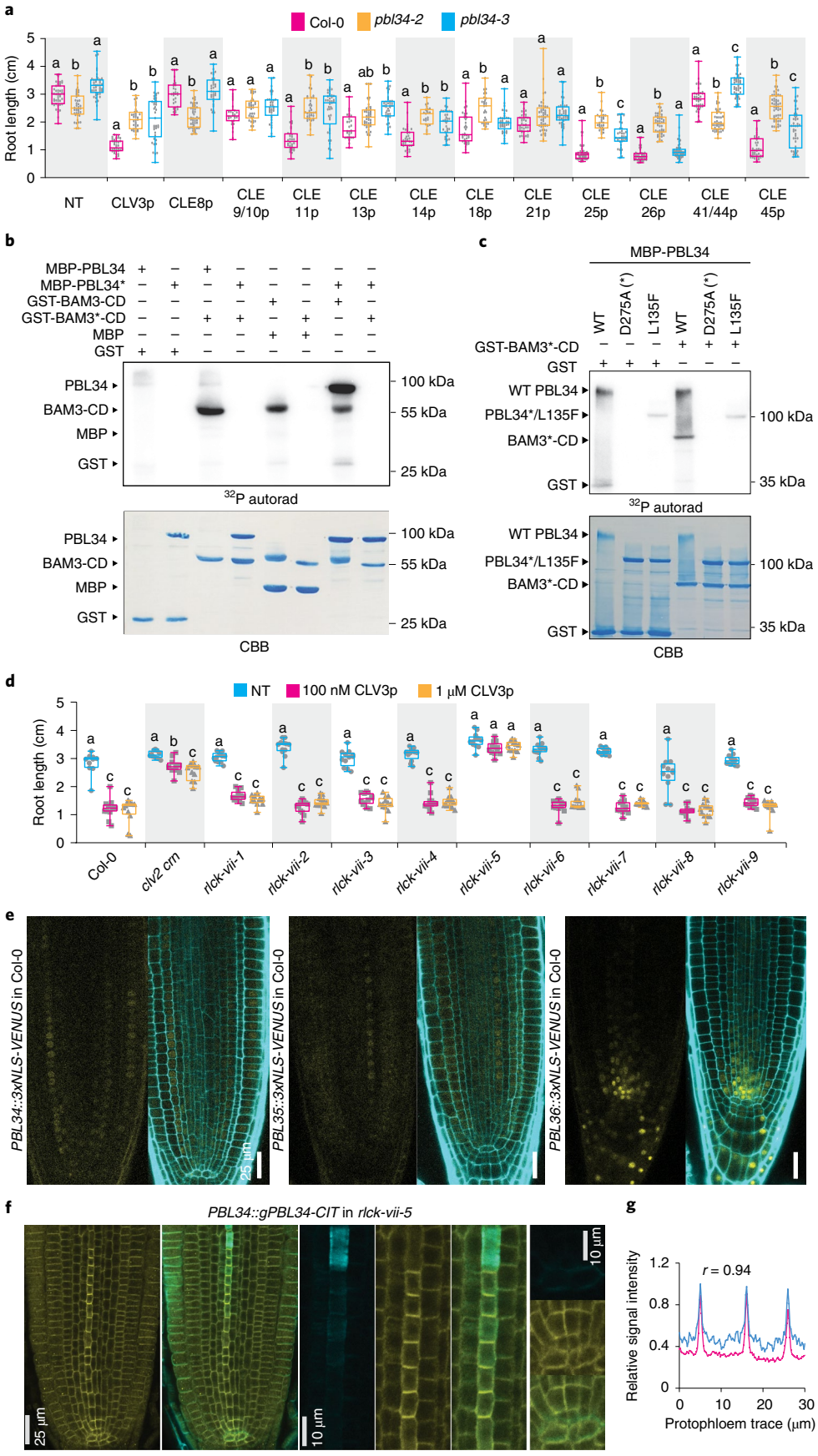
a
Col-0
pbl34-2
pbl34-3
Root length (cm)
NT
CLV3p
CLE8p
CLE 9/10p
CLE 11p
CLE 13p
CLE 14p
CLE 18p
CLE 21p
CLE 25p
CLE 26p
CLE 41/44p
CLE 45p
b
MBP-PBL34
MBP-PBL34*
GST-BAM3-CD
GST-BAM3*-CD
MBP
GST
PBL34
BAM3-CD
MBP
GST
100 kDa
55 kDa
25 kDa
32P autorad
CBB
c
MBP-PBL34
WT
D275A (*)
L135F
GST-BAM3*-CD
GST
WT PBL34
PBL34*/L135F
BAM3*-CD
GST
100 kDa
35 kDa
32P autorad
CBB
d
NT
100 nM CLV3p
1 μM CLV3p
Root length (cm)
Col-0
clv2 crn
rlck-vii-1
rlck-vii-2
rlck-vii-3
rlck-vii-4
rlck-vii-5
rlck-vii-6
rlck-vii-7
rlck-vii-8
rlck-vii-9
e
PBL34::3xNLS-VENUS in Col-0
PBL35::3xNLS-VENUS in Col-0
PBL36::3xNLS-VENUS in Col-0
25 μm
f
PBL34::gPBL34-CIT in rlck-vii-5
25 μm
10 μm
10 μm
g
Relative signal intensity
r = 0.94
Protophloem trace (μm)

rlck-vii-8 polymutant (which includes loss-of-function mutations in both *BIK1* and *PBL1*) responded normally to CLEp treatment in root length assays (Fig. 2d and Extended Data Fig. 6a), indicating pathway-specific RLCK-VII dependency.

We next examined the function of the RLCK-VII-5 clade in specific CLEp-dependent processes controlled by the primary CLV1 and BAM clade LRR-RKs. Consistent with a role in primary CLEp receptor function, CLE45p inhibited protophloem differentiation in a *BAM3* (ref. [31]) and *RLCK-VII-5* dependent manner (Fig. 3a). CLE40p regulates root quiescent centre (QC) stem cell maintenance[32], where *BAM1*, *BAM2* (ref. [33]) and *RLCK-VII-5*s are expressed (Fig. 2e,f). CLE40p promoted loss of quiescence and induced QC cell divisions in WT but not in *rlck-vii-5* or *bam1 bam2* mutants (Fig. 3b,c). In shoot and floral meristems, CLV3p and highly redundant CLE peptides signal through CLV1 and BAM receptors to limit stem cell proliferation[23,34] and disruption of CLV3p/CLEp signalling thereby results in increased floral organ numbers. Consistent with a general role of RLCK-VII-5s in CLEp perception, *rlck-vii-5* mutants also displayed a mildly increased carpel number, which was never observed in WT plants; this *rlck-vii-5* phenotype was dramatically enhanced in a sensitized *clv1* mutant background (Fig. 3d,e). Collectively, these data demonstrate that RLCK-VII-5s are critical for diverse CLEp-CLV1/BAM developmental outputs.

The roles of specific RLCK-VII family members in immune or CLEp signalling suggests that these LRR-RK pathways use similar but genetically distinct signalling components. Interestingly, while PLL4 and PLL5 regulate immunity, *pol* and *pll1* mutants were first identified as partial suppressors of *clv1* (refs. [35,36]), suggesting that they negatively regulate CLEp signalling. Ectopic QC divisions were observed in *pol* single mutants in the absence of CLE40p (Fig. 3b,c), phenocopying CLEp treatment in WT plants. We observed no such CLE-related phenotypes in *pll4 pll5* mutants (Extended Data Fig. 6a-c), whereas *pol-6* and *pll1-1* displayed WT ROS production upon flg22 or elf18 treatment (Extended Data Fig. 6d), together indicating that, as with RLCK-VII/PBLs, immune and CLEp signalling pathways use specific PLL family members.

The clustered S-X-X-L domain phosphosites identified in PLL4 are highly conserved across the PLL family (Extended Data Fig. 2) and database interrogation revealed phosphorylation at seven tandem sites within this region of POL (Fig. 4a). Given the similar roles of POL, PLL1 and PBL34 in CLEp signalling to those of PLL4, PLL5 and BIK1, PBL1 in PTI, we reasoned that the regulatory mechanisms could be conserved. To test this, we performed in vitro kinase assays with recombinant MBP-tagged POL fragments and confirmed that PBL34 directly phosphorylates the N termini of POL and PLL1 (Fig. 4b and Extended Data Fig. 7a,b). As with PLL4 and BIK1, we performed phosphosite identification via MS on MBP-POL following kinase assays with PBL34 and confirmed that PBL34 primarily phosphorylates POL within its S-X-X-L domain (Extended Data Fig. 7c). While the PBL34-targeted POL S-X-X-L sites represent bona fide phosphosites (given their presence in publicly available *Arabidopsis* datasets; Extended Data Fig. 2d), due to expression in limited tissues and endogenous CLEp signalling we were, however, unable to test whether CLEp perception triggers POL or PLL1 phosphorylation in planta. Nevertheless,

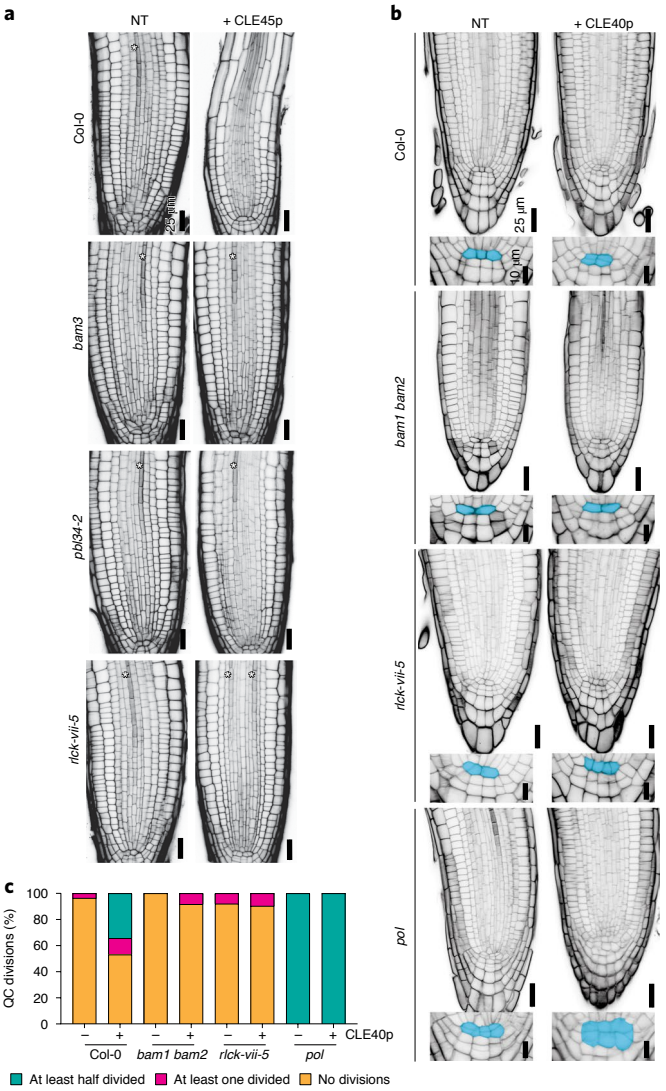

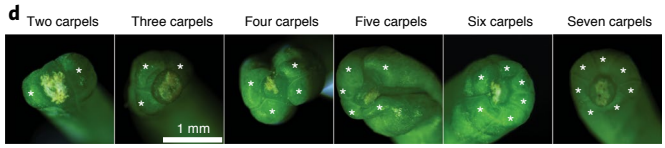

e

Genotype	Average number of carpels per flower: Carpels	s.d.	*n*	Percentage distribution of carpels per flower: 2	3	4	5	6	7
Col-0	2.00	± 0.00	803	100	0	0	0	0	0
rlck-vii-5	2.02	± 0.15	799	98.1	1.8	0.1	0	0	0
clv1	3.23	± 0.73	830	18.3	41.0	40.8	0	0	0
rlck-vii-5 clv1	3.84	± 1.11	824	14.1	22.2	34.7	23.6	5.1	0.2

Fig. 3 | The RLCK-VII-5 subfamily functions downstream of multiple primary CLEp receptors. a, RLCK-VII-5 kinases control phloem differentiation through CLE45p/BAM3 signalling pathway. Representative confocal images of 5-day-old-seedling meristems ($n \geq 15$ independent biological replicates). In *pbl34* mutants differentiated phloem files could be observed frequently, which was never observed in Col-0 WT. Mutants *bam3* and *rlck-vii-5* are CLE45p-resistant. White asterisks, phloem cell files. **b**,**c**, RLCKV-VII kinases control CLE40p/BAM1/BAM2/POL-mediated QC division. CLE40p triggers QC division dependent on RLCK-VII-5 kinases and BAM1 BAM2; while untreated *pol* displays ectopic QC divisions mimicking CLE40p treatment. **b**, Representative pictures of confocal microscopy of 5-day-old seedlings treated or not with 100 nM CLE40p. Black, Calcofluor white cell wall staining. **c**, Corresponding quantification of QC division phenotypes in control or 100 nM CLE40p-treated plants. $n = 15$–32 independent biological replicates. **d**,**e**, *rlck-vii-5* mutants display a mild extra carpel phenotype by itself and enhance the *clv1* single mutant. **d**, Representative images of carpels per flower with white asterisk indicating a carpel. **e**, Table showing the average number of carpels per flower (± s.d.) for every flower on the primary inflorescence of 30 individual 6-week-old plants per genotype and the percentage distribution of carpel number per flower.

PBL34-mediated in vitro trans-phosphorylation of the POL N terminus was lost when seven S-X-X-L motif sites were mutated to phospho-dead variants (POL-N^{7A}) (Fig. 4b), further confirming that PBL34 specifically phosphorylates the N-terminal S-X-X-L domain of POL. Furthermore, as with PLL4 in immunity, we observed that a phosphomimetic variant of POL (POL^{7D}) was compromised in association with both BAM3 (Fig. 4c) and CLV1 (Extended Data Fig. 7d) in planta, as well as showing reduced direct interaction with BAM3-CD in vitro (Extended Data Fig. 7e). POL is a plasma membrane-associated protein owing to its *N*-myristoylation, which can be blocked by a G2A mutation[37]. As with PLL4, the S-X-X-L phosphosites did not affect the plasma membrane association of POL (Extended Data Fig. 7f).

To probe the role of POL phosphorylation in CLEp-mediated development, we transformed *pol pll1*$^{-/+}$ null mutants with WT or mutant *POL* variants under the native *POL* promoter and isolated viable *pol pll1* double mutants to determine ability to complement their seedling lethal phenotype[38]. Consistent with a negative regulatory role for S-X-X-L sites, POL and POL^{7A} but not POL^{7D} complemented *pol pll1*, whereas POL^{7D} lines displayed gain-of-function *CLV3*-phenotypes across plant tissues and developmental stages and in multiple independent transgenic lines (Fig. 4d and Extended Data Fig. 8). The increased carpel number of *clv* mutants can be reverted in combination with *pol* or *pll1* single mutants[38], in which BAM RKs are still present. We observed that WT POL fully complemented this reversion in a *clv1-15 pol-6* background, whereas POL^{7D} had no effect on carpel number, as expected (Fig. 4e). Complementation with POL^{7A}, by contrast, caused a quantitative increase in carpel number (Fig. 4e), further confirming that N-terminal phosphorylation negatively regulates POL function in CLV1/BAM signalling.

Together, our data reveal a conserved regulatory circuit that controls LRR-RK signalling in both immunity and development (Fig. 4f), in which specific PLL family phosphatases and RLCK-VII/PBL family kinases control the activation of ligand-binding receptors in distinct pathways. Members of multiple RLCK families function downstream of RK complexes in immunity[12] and the RLCK-VIII family member MAZZA was recently reported to contribute to signalling downstream of CLEp perception[39]. Distinct RLCK-VIIs have also been identified downstream of LRR-RKs in other developmental processes, such as SCHENGEN 1 (SGN1)/PBL15, which functions downstream of the receptor GASSHO1(GSO1)/SGN3 to regulate Casparian strip formation[40], further indicating that LRR-RKs share conserved signalling modules downstream of receptor activation. In addition to their roles reported here, RLCK-VII-5s were also reported

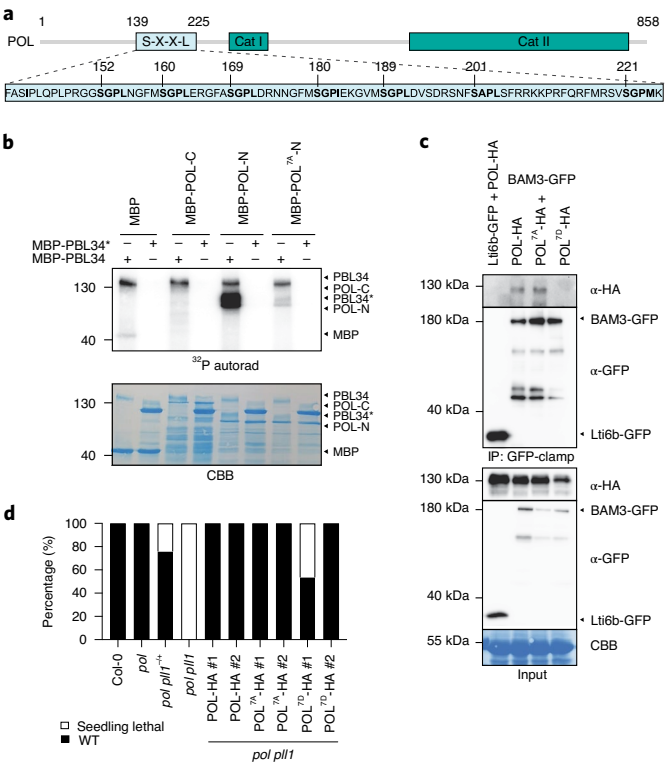

e

Genotype	Average number of carpels per flower			Percentage distribution of carpels per flower			
	Carpels	s.d.	*n*	2	3	4	5
Col-0	2.00	± 0.00	90	100	0	0	0
pol-6	2.00	± 0.00	90	100	0	0	0
clv1-15	3.20	± 0.80	90	23.3	33.3	43.3	0
clv1-15 pol-6	2.41	± 0.49	90	58.9	41.1	0	0
clv1-15 pol-6 POL-HA #1	3.00	± 0.81	90	32.2	35.6	32.2	0
clv1-15 pol-6 POL^{7A}-HA #1	3.82	± 0.57	90	2.2	20	71.1	6.7
clv1-15 pol-6 POL^{7D}-HA #1	2.11	± 0.32	90	88.9	11.1	0	0

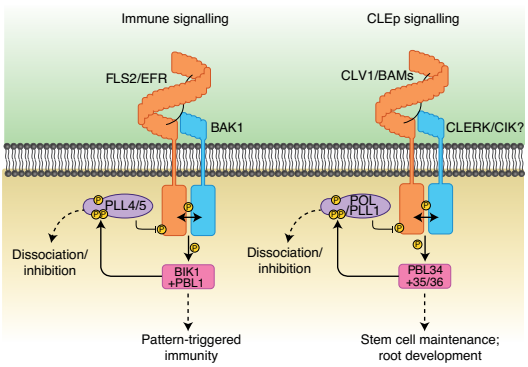

Fig. 4 | Conservation of the regulatory mechanism in PAMP and CLEp receptor complexes. a, Schematic representation of POL domains and details of the S-X-X-L domain of POL. Bold amino acids indicate the S-X-X-L residues targeted for mutagenesis in POL^{7A} or POL^{7D}; numbers correspond to the amino acid positions within the protein. **b**, PBL34 phosphorylates the POL N terminus in a site-specific manner. Autoradiogram of in vitro kinase assay of MBP-tagged C-terminal (C), N-terminal fragments of WT POL (POL-N) or phospho-dead variant (POL-N^{7A}) with WT PBL34 or inactive (PBL34*). Kinase assays were performed twice with similar results. **c**, BAM3 and POL interact in planta. CoIP assay of transiently expressed BAM3-GFP and HA-tagged WT POL, POL^{7A} or POL^{7D} variants in *N. benthamiana* leaves. CBB, Coomassie brilliant blue. Experiments were performed three times with similar results. **d**, Quantification of the complementation of *pol pll* phenotype in the shoot by POL^{7A} and POL^{7D} variants. POL-HA and POL^{7A}-HA fusion proteins fully complement the seedling lethality of the *pol pll1* double mutant. POL^{7D}-HA protein fusion only partially rescues the seedling lethality phenotype. $n \geq 117$ independent biological replicates (seedlings) per genotype. **e**, S-X-X-L phosphosites negatively regulate POL function in the sensitized *clv1-15 pol-6* background. Table shows the average number of carpels per flower (± s.d.) for every flower on the primary inflorescence of individual 6-week-old plants for each genotype and the percentage distribution of carpel number per flower ($n = 90$ flowers per genotype). **f**, Schematic representation of the conserved signalling mechanism between PTI and CLEp signalling pathways exemplified by FLS2 and BAM3 signalling pathways. In the absence of the ligand, PLL family phosphatases dampen signalling by inhibiting RK phosphorylation (for example, PLL4,5 or POL,PLL1). Perception of the apoplastic peptide ligands (for example, PAMPs or CLEps) by their cognate RKs leads to co-receptor recruitment and activation of specific RLCK-VII members. These RLCK-VII/PBLs phosphorylate PLLs at conserved N-terminal sites, negatively regulating PLLs and promoting their dissociation from the RK complex and appropriate activation of signalling.

to function downstream of LIPOOLIGOSACCHARIDE-SPECIFIC REDUCED ELICITATION (LORE)[41], a G-lectin type RK that triggers immunity in response to bacterial 3-OH-FAs[42]. It will be of interest to see if these additional RK pathways may also be regulated by a similar molecular circuitry.

Methods

Plant growth and materials. All the mutants investigated in this study are in the *A. thaliana* Col-0 WT background. Col-0 was used as the control for the phenotypic analyses. The allele named *pbl34-2* in this manuscript carries a C to T point mutation in *PBL34* (At5g15080), which leads to the substitution of leucine 135 by phenylalanine. The *pbl34-3* (SALK_126209), *pol-6* (SALK_009469.29.99.f), *pll1-1* (SAIL_319_C08), *clv1-15* (WiscDsLox489-492B1), *bam1-4* (SALK_107290), *bam2-4* (SAIL_1053_E09), *pll4* (SALK_203257C), *pll5* (SALK_044162C), *pll4-1 pll5-1* double mutants were obtained from stock centres or described before[14]. Higher order *rlck-vii* seed stocks were previously described[29]. Unless otherwise detailed, *Arabidopsis* plants were grown in a controlled environment growth chamber at 150 µmol light intensity, 60% relative humidity and 20 °C in a 10 h light cycle. *N. benthamiana* plants were grown in a controlled environment chamber at 120 µmol light intensity, 45–60% relative humidity and 19–21 °C in a 12 h light cycle.

CLEp-induced root growth inhibition assays. Seeds were sterilized, sown on half-strength Murashige and Skoog (½ MS) media supplemented with 0.3% sucrose and 1% agar, stocked at 4 °C for 48 h and grown vertically under continuous light of 120 µmol m^{-2} s^{-1} intensity at 22 °C. Synthetic CLE peptides were obtained from a commercial supplier (Genscript) at >80% purity, diluted in sterile water and used at the indicated concentration. Root lengths were measured on 600 dpi scans of the plates with Fiji software[43] using the Simple Neurite Tracer plug-in[44].

CLV3 peptide root elongation assay. Seeds were sterilized for 10 min in 70% ethanol with 0.1% Triton X-100, rinsed in 70% ethanol three times, plated onto ½ MS (MS-Research Products International), pH 5.7 with 8 g of Phytoagar (RPI) per litre. Seeds were stratified for 48 h at 4 °C. After stratification, seeds were germinated horizontally, under continuous light in a Percival growth chamber set to 22 °C for 4 d. Seedlings at 4 d after germination (DAG) were transferred to vertical ½ MS plates with or without CLV3 peptide (>95% purity, Biomatik) for mock and peptide treatment, respectively. Seedlings on vertical plates were allowed to grow for 4 d after transfer, then were scanned and measured using ImageJ software.

Phenotypic analysis of QC response to peptide. Sterilized seeds were plated onto ½ MS (MS-Research Products International), pH 5.7 with 8 g of Phytoagar (RPI) per litre with or without CLE40p peptide (>95% purity, Biomatik) for peptide and mock treatment, respectively. They were stratified for 48 h at 4 °C and grown until 5 DAG before imaging. The 5 DAG seedlings were stained for 5 min in ClearSee solution[45] containing 0.1% Calcofluor white (ChemCruz) and stained roots were dissected and mounted in ClearSee solution. Roots were observed on a Zeiss 710 inverted confocal microscope and scored into categories. Calcofluor white was excited with 405 nm and emission was collected from 410 to 551 nm.

Cloning. Polymerase chain reaction (PCR) products were amplified from plant DNA or plasmid templates (ABRC) using primers listed in Supplementary Table 1. Mutations were generated using DpnI-mediated, site-directed mutagenesis using primers listed in Supplementary Table 1. For Gateway cloning, PCR products were successively transferred to pDONR vectors by BP reaction (Invitrogen) and pDEST by LR reaction (Invitrogen) according to the manufacturer's protocols. *pPBL34::gPBL34-CIT* was cloned by Gibson strategy (NEB) into a modified pCAMBIA1305,1 plasmid carrying a FASTRED seed selection marker. *POL*, *PLL1*, *PLL4* and *PBL34* fragments were cloned into pOPINM using InFusion (Takara). The *PBL34* promoter was cloned by restriction enzyme cloning into a modified pCAMBIA1305,1 carrying a 3xNLS-VENUS cassette. The *PBL35* and *PBL36* promoters were introduced into a pCAMBIA1305,1 3xNLS-VENUS by Gibson cloning (NEB). The *POL* native promoter (3.6 kb 5′, 1.0 kb 3′) was integrated into the pMOA34 binary gateway destination vector via PCR and standard restriction cloning. For transient localization experiments in *N. benthamiana*, *POL* or *PLL4* variants were cloned behind the *35S* promoter binary vector and *N*-myristoylatable *mTurquoise2* was cloned into behind the *Ubiquitin10* promoter binary vector.

Plant transformation. Binary vectors were introduced into *Arabidopsis* via *Agrobacterium tumefaciens*-mediated (strain GV3101 *pMP90*) transformation by standard floral dipping. Transgenic lines were selected on hygromycin selection media (35 mg l^{-1}) or FASTRED seed expression. Single insertion lines were studied.

***pbl34-2* mutant isolation.** *pbl34-2* mutants were isolated as described[27]. CLE26p insensitivity was confirmed in the M_3 generation and resistant plants were backcrossed to Col-0. The F_1 was uniformly insensitive to CLE26p treatment, suggesting the dominance of this allele. The causative mutation was mapped by whole-genome sequencing of a bulk of 100 seedlings resistant to CLE26p versus 100 sensitive ones as described previously[46].

Genotyping. The *pbl34-2* mutation was genotyped with a CAPS strategy. A 730 bp PCR product was amplified with the Phire kit (Thermo Fisher). The subsequent PCR product was digested with AflII restriction enzyme, which cuts the WT product into 340 bp + 390 bp fragments but not the *pbl34-2* product. Primers for genotyping are listed in Supplementary Table 2.

Protein alignment and phylogenic tree. Protein alignments were performed using CLUSTALW (https://www.ebi.ac.uk/Tools/msa/clustalo/). The output file was uploaded into MEGA X software (https://www.megasoftware.net/) to generate the corresponding phylogenic trees.

Statistical analyses. Statistical analyses were performed on RStudio software (www.rstudio.com/) or on Prism software (https://www.graphpad.com/scientific-software/prism/). Analyses of variance (ANOVA) followed by Tukey tests were performed with a confidence level of 95%. Specific tests used are indicated in figure captions.

Recombinant protein expression and purification. All proteins were expressed in *Escherichia coli* strain BL21(DE3) Rosetta pLysS unless otherwise noted. BIK1 or BIK1* (kinase dead, K105A/K106A), PLL4, POL, PLL1 and PBL34 variants expressed as 6xHis-MBP fusion proteins in the pOPINM vector. The EFR cytosolic domain was expressed using pMAL-c4E (MBP-EFR-CD or kinase dead MBP-EFR*-CD, D849N) in BL21(DE3) Rosetta pLysS or pET-28a(+) (6xHis-EFR-CD) in BL21(DE3)-VR2-pACYC-LamP *E. coli*, respectively. The cytosolic domain of BAM3 WT or kinase dead (BAM3*, D836N) was cloned into a modified pET-28a(+) backbone and expressed as a 6xHis-GST fusion protein (GST-BAM3-CD). All proteins were purified using amylose resin (NEB) or HisPur cobalt resin (Thermo) for MBP or 6xHis, 6xHis-MBP and 6xHis-GST fusions, respectively.

In vitro kinase assays. Approximately 1 µg of kinase was incubated with ~1 µg of substrate protein in kinase buffer (25 mM Tris-Cl pH 7.4, 5 mM $MnCl_2$, 5 mM $MgCl_2$, 1 mM dithiothreitol). Reactions were initiated by addition of 5 µM ATP plus 0.5 µCi ^{32}P-γ-ATP in a final reaction volume of 30 µl. Reactions were carried out at 25 °C for 30 min and stopped by addition of SDS-loading dye and heating at 70 °C for 10 min. Proteins were resolved by SDS–polyacrylamide gel electrophoresis (SDS–PAGE), transferred to polyvinylidene fluoride (PVDF) membrane and stained with Coomassie brilliant blue G-250. Autoradiographs were imaged using an Amersham Typhoon Phosphorimager (GE Healthcare). For non-radioactive autophosphorylation of EFR, ~10 µg of MBP-EFR-CD was incubated in kinase buffer (as above) with 10 µM ATP in a final volume of 100 µl for 1 h at 25 °C. Free ATP was removed by equilibration into storage buffer (25 mM Tris-Cl pH 7.4, 100 mM NaCl, 10% glycerol, 1 mM dithiothreitol) using a 10,000 MWCO centrifugal filtration device (Millipore). For analysis by MS, in vitro kinase assays were performed as above without the addition of ^{32}P-γ-ATP.

In vitro phosphatase assays. Approximately 1 µg of autophosphorylated MBP-EFR-CD was mixed with ~1 µg of phosphatase in buffer (HEPES pH 6.8, 5 mM $MgCl_2$, 5 mM $MnCl_2$, 200 mM NaCl, 5% glycerol, 1 mM dithiothreitol). Reactions were carried out for 90 min at 25 °C. Phosphorylation was monitored by blotting with anti-pThr (anti-phosphothreonine, Cell Signalling Technology 9381, diluted 1:1,000 in TBST-5% gelatin from cold water fish skin).

ROS production assays. ROS burst assays were conducted as previously described[10,47]. For assays with *N. benthamiana*, leaf discs were harvested 2 d after infiltration and equilibrated overnight in sterile water and used for assays at 3 d after infiltration. For kinetic analyses, RLUs were collected in 30 s intervals for 60 min. T_{max} RLU was defined as the interval with the highest total value.

Transient expression. Leaves of 4-week-old *N. benthamiana* leaves were infiltrated with *A. tumefaciens* carrying constructs as indicated in figure captions. In all cases, cultures were co-infiltrated with *A. tumefaciens* carrying a P19 suppressor of gene silencing construct.

Protein extraction and co-immunoprecipitation. For co-immunoprecipitation, *N. benthamiana* leaves were detached and bisected 2 d post-infiltration. Leaf halves were equilibrated in liquid MS 1% sucrose (1–2 h) and subsequently vacuum infiltrated with MS or MS + PAMP as indicated in figure captions. Tissue was frozen and ground in liquid nitrogen. Protein extraction and immunoprecipitation were performed as described previously[10] using GFP-trap (Chromotek) or GFP-clamp[48] resin, as indicated. Proteins were separated by SDS–PAGE and blotted onto PVDF membrane. Membranes were blocked and probed in TBST-5% non-fat milk using anti-GFP (HRP-conjugated B-2, sc-9996 HRP, Santa Cruz, 1:5,000 dilution) or anti-HA (HRP-conjugated, 12013819001, Roche, 1:3,000 dilution).

For flg22-induced PLL4-HA bandshift, extractions were performed as above. Extracts were then diluted into 1× phosphatase buffer (HEPES pH 6.8, 5 mM $MgCl_2$, 5 mM $MnCl_2$, 200 mM NaCl, 5% glycerol) with or without 200 units of

λPPase (NEB) and incubated for 40 min at room temperature. Samples were then analysed by western blot as described above.

For detection of POL-HA from *POL::POL-HA* lines, tissue from 20 8-day-old seedlings grown on ½ MS was flash frozen in liquid nitrogen and protein extraction was performed as above. Proteins were separated by SDS–PAGE (4–12% Bolt Gel run in 1× Bolt MOPS SDS running buffer from Thermo) and transferred to PVDF membrane. Membranes were blocked and probed in TBST-4% non-fat milk using anti-HA as primary (Clone 3F10, Roche, 1:1,000 dilution) and anti-rat HRP-conjugated as secondary (polyclonal antibody, Santa Cruz Biotech, 1:5,000 dilution).

Sample preparation for mass spectrometry. Affinity-purified protein samples were separated on a 4–12% NuPAGE gel (Invitrogen). The gel was stained with InstantBlue (abcam) and the band corresponding to MBP-PLL4* or MBP-POL* was excised, cut into smaller pieces and washed three times with 50% acetonitrile, 50 mM ammonium bicarbonate (50% AcN/ABC), 30 min each, followed by dehydration in acetonitrile, 10 min. Gel pieces were then reduced with 10 mM dithiothreitol for 30 min at 45 °C followed by alkylation with 55 mM iodoacetamide for 20 min at room temperature and a further three washes with 50% AcN/ABC, 30 min each. Gel pieces were dehydrated again with acetonitrile before rehydration with 40 µl of trypsin (Pierce Trypsin Protease, MS-Grade, catalogue no. 90058) working solution (100 ng of trypsin in 50 mM ammonium bicarbonate, 5% (v/v) acetonitrile). Where required, gel pieces were covered with 50 mM ammonium bicarbonate to a final volume before incubation at 37 °C overnight. Tryptic peptides were extracted from the gel pieces three times in an equal volume of 50% acetonitrile, 5% formic acid (Pierce LC–MS-Grade, catalogue no. 85178), 30 min each. Extracted peptides were dried in a speed-vac and resuspended in 2% acetonitrile/ 0.2% trifluoroacetic acid (Merck, catalogue no. 302031). A total of four biological replicates for each sample type were submitted.

LC–MS/MS analysis. Approximately 35% of each sample was analysed using an Orbitrap Fusion Tribrid Mass Spectrometer (Thermo Fisher Scientific) coupled to a U3000 nano-UPLC (Thermo Fisher Scientific). The dissolved peptides were injected onto a reverse phase trap column NanoEase *m/z* Symmetry C18, beads diameter 5 µm, inner diameter 180 µm × 20 mm length (Waters). Trap column flow rate was 20 µl min^{-1} in 2% acetonitrile, 0.05% TFA. Peptides were eluted from trap column onto the analytical column NanoEase *m/z* HSS C18 T3 Column, beads diameter 1.8 µm, inner diameter 75 µm × 250 mm length (Waters). The column was equilibrated with 3% B (B, 80% acetonitrile in 0.05% formic acid (FA); A, 0.1% FA) before subsequent elution with the following steps of a linear gradient: 2.5 min 3% B, 5 min 6.3% B, 13 min 12.5% B, 50 min 42.5% B, 58 min 50% B, 61 min 65% B, 63 min 99% B, 66 min 99% B, 67 min 3% B, 90 min 3% B. The flow rate was set to 200 nl min^{-1}. The mass spectrometer was operated in positive ion mode with nano-electrospray ion source. Molecular ions were generated by applying voltage +2.2 kV to a conductive union coupling the column outlet with fused silica PicoTip emitter, ID 10 µm (New Objective) and the ion transfer capillary temperature was set to 275 °C. The mass spectrometer was operated in data-dependent mode using a full scan, *m/z* range 300–1,800, nominal resolution of 120,000, target value 1×10^6, followed by MS/MS scans of the 40 most abundant ions. MS/MS spectra were acquired using normalized collision energy of 30%, isolation width of 1.6 *m/z*, resolution of 120,000 and a target value set to 1×10^5. Precursor ions with charge states 2–7 were selected for fragmentation and put on a dynamic exclusion list for 30 s. Multistage activation was applied for detection of −98, −49 or −32.7 from the precursor (corresponding to the neutral loss of phosphoric acid from +1, +2 and +3 charge states, respectively) during any of the MS/MS scans. The minimum automatic gain control target was set to 5×10^3 and intensity threshold was calculated to be 4.8×10^4. The peptide match feature was set to the preferred mode and the feature to exclude isotopes was enabled.

Data processing and peptide identification. Peak lists in the form of Mascot generic files were prepared from raw data files using MS Convert (Proteowizard) and sent to a peptide search on Mascot server v.2.7 using Mascot Daemon (Matrix Science) against an in-house constructs and contaminants database and the *E. coli* K12 protein database. Tryptic peptides with up to one possible miscleavage and charge states +2 and +3 were allowed in the search. The following peptide modifications were included in the search: carbamidomethylated cysteine (fixed), oxidized methionine (variable) and phosphorylated serine, threonine and tyrosine (variable). Data were searched with a monoisotopic precursor and fragment ion mass tolerance 10 ppm and 0.8 Da respectively. Decoy database was used to validate peptide sequence matches. Mascot results were combined in Scaffold v.4.4.0 (Proteome Software) and filtered to show only phosphopeptides. Peptide and protein identifications were accepted if peptide probability and protein threshold was ≥80.0% and 99% respectively. Data were then exported to Excel (Microsoft) for further processing. For each phosphopeptide, spectral counts from all biological replicates were summed. Spectral counts from miscleaved peptides identifying the same phosphorylation site were then summed to give final spectral counts for each site.

In vitro pulldowns. Approximately 6 µg each of bait and prey proteins were mixed to 100 µl of final volume in buffer (25 mM Tris-Cl pH 7.4, 100 mM NaCl, 0.2% Triton X-100, 1 mM dithiothreitol). A total of 30 µl was removed ('input') and the remaining sample was mixed with 50 µl of amylose resin (NEB) in a final volume of 500 µl. Samples were mixed at room temperature for 30 min. The resin was washed three times with buffer and enriched proteins were eluted with 50 µl of SDS-loading dye ('pulldown'). Samples were separated by SDS–PAGE, transferred to PVDF and imaged by blotting with anti-polyhistidine (Sigma H1029), anti-GST (Upstate 06332) or anti-MBP (NEB E8032) (all diluted 1:10,000 in TBST-5% non-fat milk powder).

Confocal microscopy. The 5–6-day-old seedlings were imaged using an SP8 (Leica) inverted confocal microscope. Samples were prepared in a drop of 0.04 mg ml^{-1} propidium iodide solution. CITRINE (CIT) and VENUS fluorophores were exited at 514 nm and emitted light recorded between 520 and 555 nm. Propidium iodide was excited at 488 and 514 nm and fluorescent light recorded between 600 and 700 nm. CIT/VENUS and propidium iodide channels were sequentially acquired. For localization in *N. benthamiana*, mYPet (POL) or eYFP (PLL4) and mTurquoise2 controls were excited at 514 and 458 nm, respectively, and emitted light recorded between 516–593 nm and 460–520 nm, respectively, on a Zeiss 710 confocal microscope. Localization controls and single transformed cells were used to exclude channel bleed through. Figures were prepared using Fiji software or Zen (Zeiss). PBL34-CIT shoot apical meristem images were acquired on a Zeiss 710 with an InverterScope attachment as described in ref. [49]. CIT and chlorophyll were excited at 514 nm and emitted light recorded for CIT (519–548 nm) and chlorophyll (602–728 nm).

Immunolocalization. The 5-day-old seedlings of transgenic line expressing *pPBL34::gPBL34-CIT* in the *rlckv-vii-5* background were used for whole mount immunolocalization of the PBL34-CIT protein fusion as described previously[50] and combined with Calcofluor white cell wall staining. Primary anti-GFP rabbit (Abcam) was used at 1:600 and secondary Alexa Fluor 546 anti-rabbit was used at 1:500 (Molecular Probes).

Carpel counts. Genotype-confirmed seeds were sterilized, stratified and germinated as above. Seedlings (4 DAG) were transplanted to soil (seven parts top soil to one part sand with pesticide) and kept at high humidity for 3–5 d under continuous 24 h light at 23 °C. Seedlings were removed from high humidity and allowed to grow to full maturity, with gentle staking to prevent tangling at ~3 weeks after transplant. After 5 weeks of growth, the entire number of flowers produced on the primary inflorescence were quantified for carpel number under a dissecting microscope. Data were analysed in PRISM as above.

Isolation of *POL* complementation lines. *POL* constructs were introduced into *pol-6 pll1-1*/+ line and transgene fixed lines were isolated in the *pol-6 pll1-1* background (or *pol-6 pll1-1*/+ if necessary). Fixed lines were used for complementation analysis and expression analysis. Initial complementation was determined by identifying the ratio of viable to seedling lethal phenotypes for each *POL* variant. The WT and 7A lines displayed 100% viable phenotypes, while the 7D variants displayed a mixed set of phenotypic ratios. Viable 7D lines were transplanted and assayed for post-seedling stem cell defects.

Quantitative PCR. Bulk 8-day-old *pol pll1 POL::POL-HA* seedlings (12 for WT phenotype, 20 for seedling lethal phenotypes and an approximate weight mix for mixed phenotype) were ground in liquid nitrogen using SPEX Genogrinder and glass beads. The resulting powder was used as the starting material for a standard RNA extraction using a Qiagen Plant Mini Kit (Qiagen). About 1 ug of RNA from resulting extraction was used as template in standard complementary DNA synthesis reaction (BioRad iScript cDNA Synthesis Kit). A total 200 ng of resulting cDNA was used in quantitative PCR with reverse transcription reactions to quantify POL expression levels (PowerUp SYBR Green 5× Master Mix-Thermo). CDKA1 was used as an equalization housekeeping gene. Data were analysed using the ΔΔCT method for three biological replicates with three technical replicates each.

***POL* complementation analysis.** For seedling analyses, seeds of *POL* substitution lines were sterilized and plated on ½ MS plates (described above). The 8-day-old seedlings were assayed for seedling lethal *pol pll* double mutant or WT phenotype. Representative individual plants were genotyped to confirm correct genotype. For adult plant analyses, 5-day-old seedlings were transplanted to soil (as above). Plants were grown for 4–6 weeks and phenotypes were assayed accordingly.

Reporting Summary. Further information on research design is available in the Nature Research Reporting Summary linked to this article.

Data availability

Identifiers for published or publicly available lines are provided in the Methods. The mass spectrometry proteomics data have been deposited to the ProteomeXchange Consortium via the PRIDE[51] partner repository with the dataset identifier PXD031441 and https://doi.org/10.6019/PXD031441. Source data are provided with this paper. All other relevant data are available from the corresponding authors upon request.

Received: 7 February 2022; Accepted: 14 March 2022;
Published online: 14 April 2022

References

1. Hohmann, U., Lau, K. & Hothorn, M. The structural basis of ligand perception and signal activation by receptor kinases. *Annu. Rev. Plant Biol.* **68**, 109–137 (2017).
2. Dievart, A., Gottin, C., Périn, C., Ranwez, V. & Chantret, N. Origin and diversity of plant receptor-like kinases. *Annu. Rev. Plant Biol.* **71**, 131–156 (2020).
3. Shiu, S. & Bleecker, A. B. Expansion of the receptor-like kinase/pelle gene family and receptor-like proteins in *Arabidopsis*. *Plant Physiol.* **132**, 530–543 (2003).
4. Gómez-Gómez, L. & Boller, T. FLS2: an LRR receptor-like kinase involved in the perception of the bacterial elicitor flagellin in *Arabidopsis*. *Mol. Cell* **5**, 1003–1011 (2000).
5. Zipfel, C. et al. Bacterial disease resistance in *Arabidopsis* through flagellin perception. *Nature* **428**, 764–767 (2004).
6. Zipfel, C. et al. Perception of the bacterial PAMP EF-Tu by the receptor EFR restricts *Agrobacterium*-mediated transformation. *Cell* **125**, 749–760 (2006).
7. Liang, X. & Zhou, J. Receptor-like cytoplasmic kinases: central players in plant receptor kinase-mediated signaling. *Annu. Rev. Plant Biol.* **69**, 267–299 (2018).
8. Veronese, P. et al. The membrane-anchored BOTRYTIS-INDUCED KINASE1 plays distinct roles in *Arabidopsis* resistance to necrotrophic and biotrophic pathogens. *Plant Cell* **18**, 257–273 (2006).
9. Lu, D. et al. A receptor-like cytoplasmic kinase, BIK1, associates with a flagellin receptor complex to initiate plant innate immunity. *Proc. Natl Acad. Sci. USA* **107**, 496–501 (2010).
10. Kadota, Y. et al. Direct regulation of the NADPH oxidase RBOHD by the PRR-associated kinase BIK1 during plant immunity. *Mol. Cell* **54**, 43–55 (2014).
11. Li, L. et al. The FLS2-associated kinase BIK1 directly phosphorylates the NADPH oxidase RbohD to control plant immunity. *Cell Host Microbe* **15**, 329–338 (2014).
12. DeFalco, T. A. & Zipfel, C. Molecular mechanisms of early plant pattern-triggered immune signaling. *Mol. Cell* **81**, 3449–3467 (2021).
13. Couto, D. et al. The *Arabidopsis* protein phosphatase PP2C38 negatively regulates the central immune kinase BIK1. *PLoS Pathog.* **12**, e1005811 (2016).
14. Holton, N., Nekrasov, V., Ronald, P. C. & Zipfel, C. The phylogenetically-related pattern recognition receptors EFR and XA21 recruit similar immune signaling components in monocots and dicots. *PLoS Pathog.* **11**, e1004602 (2015).
15. Park, C.-J. et al. Rice XB15, a protein phosphatase 2C, negatively regulates cell death and XA21-mediated innate immunity. *PLoS Biol.* **6**, e231 (2008).
16. Segonzac, C. et al. Negative control of BAK1 by protein phosphatase 2A during plant innate immunity. *EMBO J.* **33**, 2069–2079 (2014).
17. Couto, D. & Zipfel, C. Regulation of pattern recognition receptor signalling in plants. *Nat. Rev. Immunol.* **16**, 537–552 (2016).
18. Yu, L. P., Miller, A. K. & Clark, S. E. POLTERGEIST encodes a protein phosphatase 2C that regulates CLAVATA pathways controlling stem cell identity at *Arabidopsis* shoot and flower meristems. *Curr. Biol.* **13**, 179–188 (2003).
19. Heazlewood, J. I. et al. PhosPhAt: a database of phosphorylation sites in *Arabidopsis thaliana* and a plant-specific phosphorylation site predictor. *Nucleic Acids Res.* **36**, 1015–1021 (2008).
20. Mergner, J. et al. Mass-spectrometry-based draft of the *Arabidopsis* proteome. *Nature* **579**, 409–414 (2020).
21. Thor, K. et al. The calcium-permeable channel OSCA1.3 regulates plant stomatal immunity. *Nature* **585**, 569–573 (2020).
22. Hazak, O. & Hardtke, C. S. CLAVATA 1-type receptors in plant development. *J. Exp. Bot.* **67**, 4827–4833 (2016).
23. Nimchuk, Z. L. CLAVATA1 controls distinct signaling outputs that buffer shoot stem cell proliferation through a two-step transcriptional compensation loop. *PLoS Genet.* **13**, e1006681 (2017).
24. Goad, D. M., Zhu, C. & Kellogg, E. A. Comprehensive identification and clustering of CLV3/ESR-related (CLE) genes in plants finds groups with potentially shared function. *New Phytol.* **216**, 605–616 (2017).
25. Fletcher, J. C. Recent advances in *Arabidopsis* CLE peptide signaling. *Trends Plant Sci.* **25**, 1005–1016 (2020).
26. Yamaguchi, Y. L., Ishida, T. & Sawa, S. CLE peptides and their signaling pathways in plant development. *J. Exp. Bot.* **67**, 4813–4826 (2016).
27. Anne, P. et al. CLERK is a novel receptor kinase required for sensing of root-active CLE peptides in *Arabidopsis*. *Development* **145**, dev162354 (2018).
28. Hazak, O. et al. Perception of root-active CLE peptides requires CORYNE function in the phloem vasculature. *EMBO Rep.* **18**, 1367–1381 (2017).
29. Rao, S. et al. Roles of receptor-like cytoplasmic kinase VII members in pattern-triggered immune signaling. *Plant Physiol.* **177**, 1679–1690 (2018).
30. Wang, W. et al. Receptor-like cytoplasmic kinases PBL34/35/36 are required for CLE peptide-mediated signaling to maintain shoot apical meristem and root apical meristem homeostasis in *Arabidopsis*. *Plant Cell* https://doi.org/10.1093/plcell/koab315 (2021).
31. Depuydt, S. et al. Suppression of *Arabidopsis* protophloem differentiation and root meristem growth by CLE45 requires the receptor-like kinase BAM3. *Proc. Natl Acad. Sci. USA* **110**, 7074–7079 (2013).
32. Stahl, Y., Wink, R. H., Ingram, G. C. & Simon, R. A signaling module controlling the stem cell niche in *Arabidopsis* root meristems. *Curr. Biol.* **19**, 909–914 (2009).
33. Crook, A. D. et al. BAM1/2 receptor kinase signaling drives CLE peptide-mediated formative cell divisions in *Arabidopsis* roots. *Proc. Natl Acad. Sci. USA* **117**, 32750–32756 (2020).
34. Rodriguez-Leal, D. et al. Evolution of buffering in a genetic circuit controlling plant stem cell proliferation. *Nat. Genet.* **51**, 786–792 (2019).
35. Yu, L. P., Simon, E. J., Trotochaud, A. E. & Clark, S. E. POLTERGEIST functions to regulate meristem development downstream of the CLAVATA loci. *Development* **127**, 1661–1670 (2000).
36. Song, S. K. & Clark, S. E. POL and related phosphatases are dosage-sensitive regulators of meristem and organ development in *Arabidopsis*. *Dev. Biol.* **285**, 272–284 (2005).
37. Gagne, J. M. & Clark, S. E. The *Arabidopsis* stem cell factor POLTERGEIST Is membrane localized and phospholipid stimulated. *Plant Cell* **22**, 729–743 (2010).
38. Song, S. K., Lee, M. M. & Clark, S. E. POL and PLL1 phosphatases are CLAVATA1 signaling intermediates required for *Arabidopsis* shoot and floral stem cells. *Development* **133**, 4691–4698 (2006).
39. Blümke, P. et al. Receptor-like cytoplasmic kinase MAZZA mediates developmental processes with CLAVATA1 family receptors in *Arabidopsis*. *J. Exp. Bot.* **72**, 4853–4870 (2021).
40. Fujita, S. et al. SCHENGEN receptor module drives localized ROS production and lignification in plant roots. *EMBO J.* **39**, e103894 (2020).
41. Luo, X. et al. Tyrosine phosphorylation of the lectin receptor-like kinase LORE regulates plant immunity. *EMBO J.* **39**, e102856 (2020).
42. Kutschera, A. et al. Bacterial medium-chain 3-hydroxy fatty acid metabolites trigger immunity in *Arabidopsis* plants. *Science* **364**, 178–181 (2019).
43. Schindelin, J. et al. Fiji: an open-source platform for biological-image analysis. *Nat. Methods* **9**, 676–682 (2012).
44. Longair, M. H., Baker, D. A. & Armstrong, J. D. Simple neurite tracer: open source software for reconstruction, visualization and analysis of neuronal processes. *Bioinformatics* **27**, 2453–2454 (2011).
45. Kurihara, D., Mizuta, Y., Sato, Y. & Higashiyama, T. ClearSee: a rapid optical clearing reagent for whole-plant fluorescence imaging. *Development* **142**, 4168–4179 (2015).
46. Kang, Y. H. & Hardtke, C. S. *Arabidopsis* MAKR 5 is a positive effector of BAM 3-dependent CLE 45 signaling. *EMBO Rep.* **17**, 1145–1154 (2016).
47. Monaghan, J., Matschi, S., Romeis, T. & Zipfel, C. The calcium-dependent protein kinase CPK28 negatively regulates the BIK1-mediated PAMP-induced calcium burst. *Plant Signal. Behav.* **10**, e1018497 (2015).
48. Hansen, S. et al. Design and applications of a clamp for Green Fluorescent Protein with picomolar affinity. *Sci. Rep.* **7**, 6292 (2017).
49. Nimchuk, Z. L. & Perdue, T. D. Live imaging of shoot meristems on an inverted confocal microscope using an objective lens inverter attachment. *Front. Plant Sci.* https://doi.org/10.17615/c3nc-5w03 (2017).
50. Marhava, P. et al. A molecular rheostat adjusts auxin flux to promote root protophloem differentiation. *Nature* **558**, 297–300 (2018).
51. Perez-Riverol, Y. et al. The PRIDE database and related tools and resources in 2019: improving support for quantification data. *Nucleic Acids Res.* **47**, D442–D450 (2019).

Acknowledgements

We thank J.-M. Zhou (CAS, Beijing) for kindly providing published *rlck-vii* mutants and P. Tarr (Caltech, USA) for the Myr-mTurquoise2 plasmid. The Nimchuk laboratory thanks T. D. Perdue, director of the University of North Carolina—Chapel Hill Genome Sciences Microscopy Core, for assistance with confocal imaging. The Zipfel group thanks all members for discussions and critical reading of the manuscript. This research was supported by the Gatsby Charitable Foundation (C.Z.), the University of Zürich (C.Z.), the European Research Council under the grant agreement nos. 309858 and 773153 (grants 'PHOSPHOinnATE' and 'IMMUNO-PEPTALK' to C.Z.), the Swiss National Science Foundation (grant agreement nos. 31003A_182625 to C.Z. and 310030B_185379 to C.S.H.), a National Institute of General Medical Sciences—Maximizing Investigators' Research Award from the NIH (R35GM119614 to Z.L.N.), the National Science Foundation (IOS-1455607 to Z.L.N.), startup funds from Virginia Tech to Z.L.N. and a joint European Research Area Network for Coordinating Action in Plant Sciences (ERA-CAPS) grant ('SICOPID') from UK Research and Innovation (BB/S004734/1 to C.Z.) and National Science Foundation (IOS-1841917 to Z.L.N.), respectively. T.A.D. and P.A. were supported by the European Molecular Biology Organization (fellowships EMBO-LTF-100-2017 to T.A.D. and EMBO-LTF-480-2016

to P.A.). T.A.D. was further supported by the Natural Sciences and Engineering Council of Canada (fellowship PDF-532561-2019). P.A. and Y.G. were also supported by a Tremplin grant from the University of Lausanne.

Author contributions

T.A.D., P.A., S.R.J., C.Z., C.S.H. and Z.L.N. were responsible for conceptualization and methodology. T.A.D., P.A., S.R.J., A.W. and F.S. undertook validation. T.A.D., P.A., S.R.J., A.W., F.S., O.J., P.D., Y.G., Q.W. and S.R. were involved in formal analysis. T.A.D., P.A., S.R.J., A.W., F.S., O.J., P.D., Y.G., Q.W., S.R., A-M.P. and Z.L.N. undertook investigation. T.A.D., P.A., S.R.J., A.W., F.S. and P.D. were involved in data curation. T.A.D., P.A. and S.R.J. wrote the original draft. T.A.D., P.A., S.R.J., C.Z., C.S.H. and Z.L.N. undertook reviewing and editing of the manuscript. T.A.D., P.A. and S.R.J. were involved in visualization. F.L.H.M., C.Z., C.S.H. and Z.L.N. undertook supervision. C.Z., C.S.H. and Z.L.N. were responsible for project administration. T.A.D., P.A., C.Z., C.S.H. and Z.L.N. acquired funding.

Competing interests

The authors declare no competing interests.

Additional information

Extended data is available for this paper at https://doi.org/10.1038/s41477-022-01134-w.

Supplementary information The online version contains supplementary material available at https://doi.org/10.1038/s41477-022-01134-w.

Correspondence and requests for materials should be addressed to Cyril Zipfel, Christian S. Hardtke or Zachary L. Nimchuk.

Reprints and permissions information is available at www.nature.com/reprints.

Publisher's note Springer Nature remains neutral with regard to jurisdictional claims in published maps and institutional affiliations.

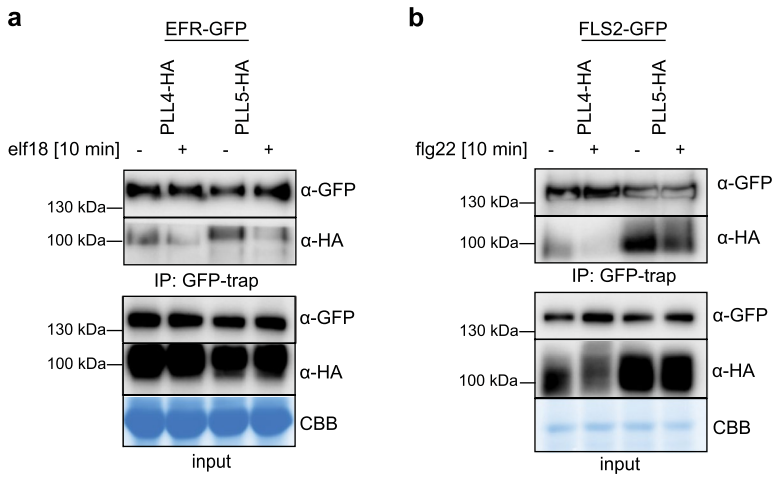

Extended Data Fig. 1 | PLL4 and PLL5 dynamically associate with EFR and FLS2 in ligand-dependent manner. (**a**) elf18 triggers EFR/PLL4,5 dissociation *in planta*. CoIP assay of transiently expressed EFR-GFP and HA-tagged PLL4 or PLL5 in *N. benthamiana* leaves with or without treatment with 1 μM of elf18 for 10 minutes. **(b)** flg22 triggers FLS2/PLL4,5 dissociation *in planta*. CoIP assay of transiently expressed FLS2-GFP and HA-tagged PLL4 or PLL5 in *N. benthamiana* leaves with or without treatment with 1 μM of flg22 for 10 minutes. CBB: Coomassie brilliant blue. Experiments were performed twice with similar results.

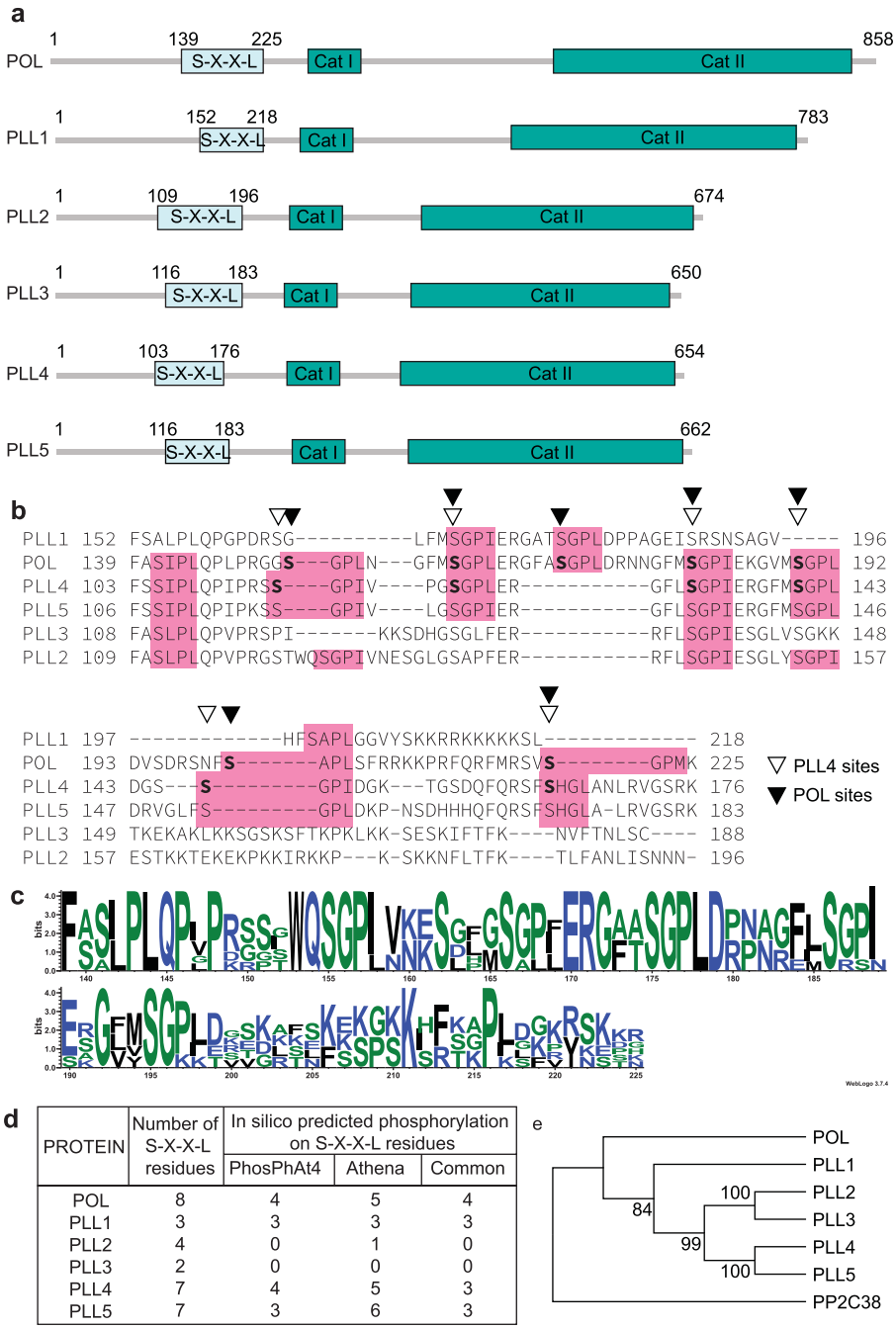

d

PROTEIN	Number of S-X-X-L residues	In silico predicted phosphorylation on S-X-X-L residues		
		PhosPhAt4	Athena	Common
POL	8	4	5	4
PLL1	3	3	3	3
PLL2	4	0	1	0
PLL3	2	0	0	0
PLL4	7	4	5	3
PLL5	7	3	6	3

e

Extended Data Fig. 2 | The S-X-X-L domain is conserved among the PLL family. (a) Schematic representation of PLLs protein domains. light blue: S-X-X-L domain, green: catalytic domains. Numbers indicates amino acid residues. **(b)** Protein alignment of the S-X-X-L domain of POL family members. Pink square: S-X-X-L residues; bold: residues targeted for mutagenesis in current study in POL (black arrow head) and PLL4 (white arrow head). **(c)** Sequence logo of the S-X-X-L domain of the POL/PLL family created from the alignment in panel B using the WebLogo3 online application (http://weblogo.threeplusone.com). **(d)** Table resuming the *in silico* predicted phosphorylation in the S-X-X-L domain identified in PhosPhAt4[19] and/or Athena databases[20]. **(e)** Phylogenetic tree of the POL family based on protein alignment. PP2C38 is used as an outgroup.

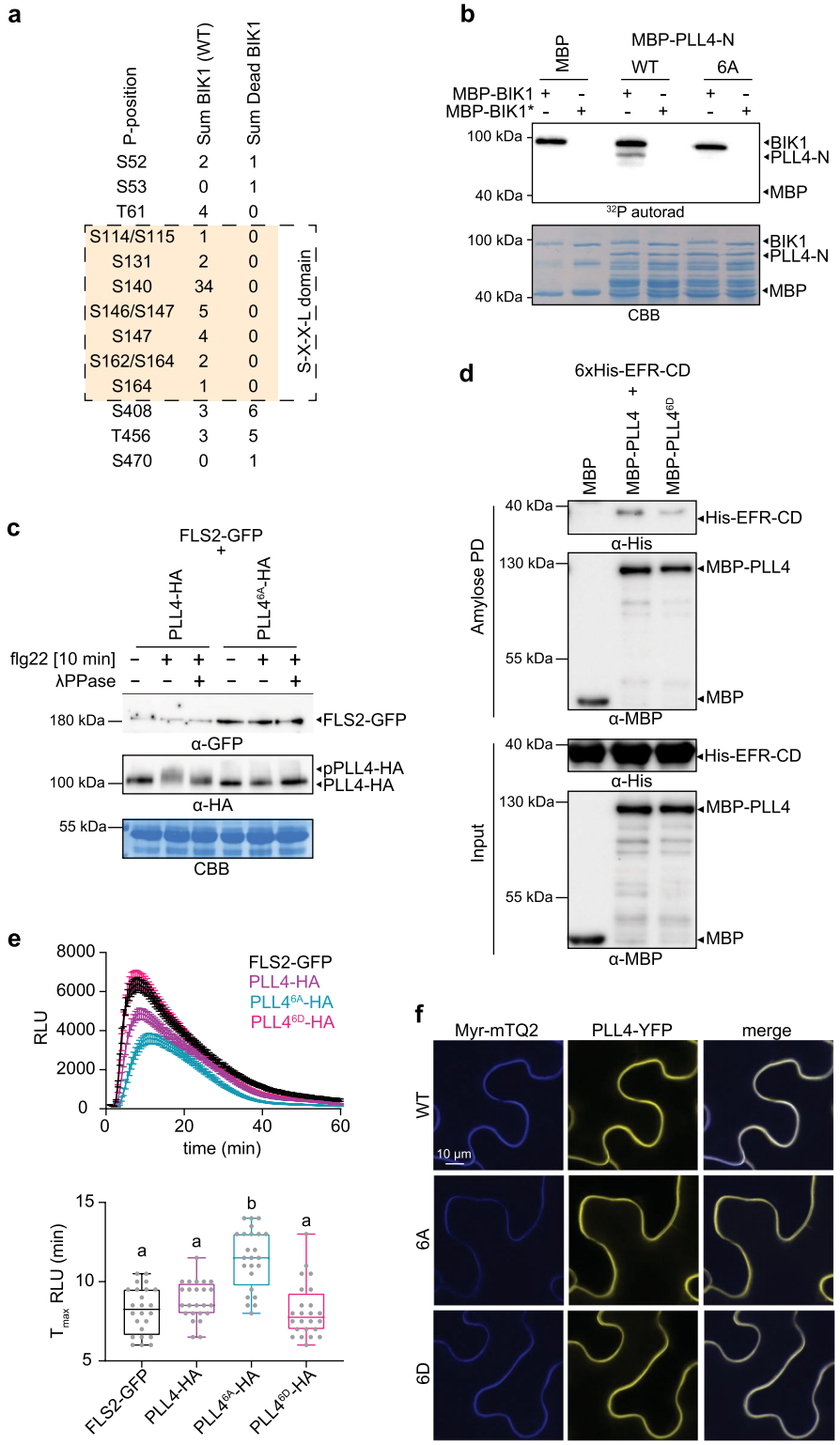

Extended Data Fig. 3 | See next page for caption.

Extended Data Fig. 3 | PLL4 regulates PTI in a phosphorylation-dependent manner. (**a**) BIK1-dependent phosphosites identified on MBP-PLL4* by LC–MS/MS following *in vitro* kinase assays. Numbers indicate sum of total spectra identified across 4 replicates corresponding to phosphorylation at the specified residue(s) in PLL4. Some spectra were ambiguous for two phosphorylation positions. Sites within the S-X-X-L domain of PLL4 are outlined and spectra corresponding to sites targeted for mutagenesis are highlighted. **(b)** BIK1 phosphorylates S-X-X-L motif sites within the PLL4 N terminus. Autoradiogram of *in vitro* kinase assay PLL4-N (WT) or PLL4^{6A}-N. Kinase assays were performed three times with similar results. **(c)** Treatment with 100 nM flg22 induces a phosphosite-dependent mobility shift in PLL4-HA. *N. benthamiana* leaves transiently expressing FLS2-GFP and PLL4-HA or PLL4^{6A}-HA were treated with or without 100 nM flg22 for 10 min prior to protein extraction, λPPase treatment, and blotting. Assays were performed three times with similar results. **(d)** PLL4 phosphomimetic (PLL4^{6D}) mutation disrupts direct interaction between PLL4 and EFR-CD *in vitro*. Amylose pulldown assay of 6xHis-tagged cytosolic domain (CD) of EFR with MBP-tagged WT version (PLL4) or phosphovariant (PLL^{6D}) of PLL4. Assays were performed three times with similar results. **(e)** Expression of PLL4^{6A} dampens PTI responses in *N. benthamiana*. ROS burst induction by elf18 (100 nM) on leaf discs of *N. benthamiana* transiently expressing FLS2-GFP and PLL4-HA variants (curves show mean values ±s.e.). Bottom panel displays the time to maximum response; letters indicate statistically different values (one-way ANOVA with Dunnett's test); n = 24 leaf discs from 3 biologically-independent leaves. Box plots show 25th to 75th percentile range with a line at the median and whiskers from minimum to maximum values. Assays were performed three times with similar results. **(f)** S-X-X-L phosphorylation does not alter accumulation of PLL4-YFP at the plasma membrane. Confocal images showing PLL4-YFP (WT or mutant variants; yellow channel) and Myr-mTQ2 (myristoylatable-mTurquoise2, PM marker; blue channel) following co-expression in *N. benthamiana* leaves.

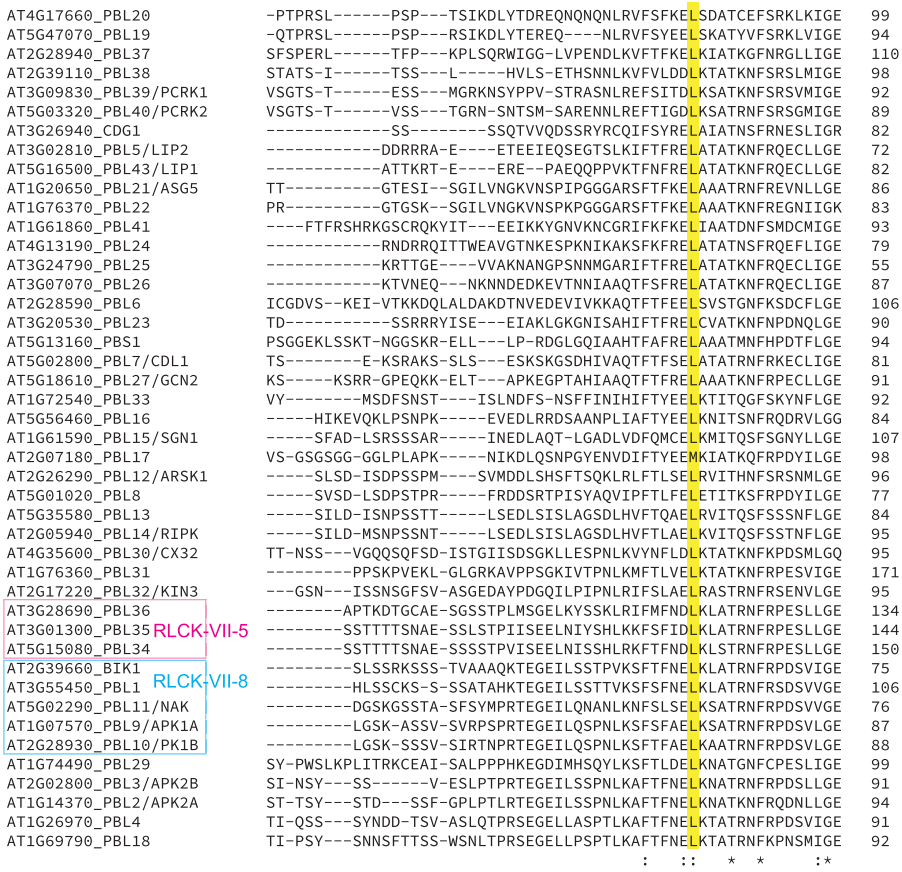


```
AT4G17660_PBL20          -PTPRSL------PSP---TSIKDLYTDREQNQNQNLRVFSFKELSDATCEFSRKLKIGE   99
AT5G47070_PBL19          -QTPRSL------PSP---RSIKDLYTEREQ----NLRVFSYEELSKATYVFSRKLVIGE   94
AT2G28940_PBL37          SFSPERL------TFP---KPLSQRWIGG-LVPENDLKVFTFKELKIATKGFNRGLLIGE  110
AT2G39110_PBL38          STATS-I------TSS---L-----HVLS-ETHSNNLKVFVLDDLKTATKNFSRSLMIGE   98
AT3G09830_PBL39/PCRK1    VSGTS-T------ESS---MGRKNSYPPV-STRASNLREFSITDLKSATKNFSRSVMIGE   92
AT5G03320_PBL40/PCRK2    VSGTS-T------VSS---TGRN-SNTSM-SARENNLREFTIGDLKSATRNFSRSGMIGE   89
AT3G26940_CDG1           ----------SS--------SSQTVVQDSSRYRCQIFSYRELAIATNSFRNESLIGR   82
AT3G02810_PBL5/LIP2      ----------DDRRRA-E----ETEEIEQSEGTSLKIFTFRELATATKNFRQECLLGE   72
AT5G16500_PBL43/LIP1     ----------ATTKRT-E----ERE--PAEQQPPVKTFNFRELATATKNFRQECLLGE   82
AT1G20650_PBL21/ASG5     TT----------GTESI--SGILVNGKVNSPIPGGGARSFTFKELAAATRNFREVNLLGE   86
AT1G76370_PBL22          PR----------GTGSK--SGILVNGKVNSPKPGGGARSFTFKELAAATKNFREGNIIGK   83
AT1G61860_PBL41          ----FTFRSHRKGSCRQKYIT---EEIKKYGNVKNCGRIFKFKELIAATDNFSMDCMIGE   93
AT4G13190_PBL24          ----------RNDRRQITTWEAVGTNKESPKNIKAKSFKFRELATATNSFRQEFLIGE   79
AT3G24790_PBL25          ----------KRTTGE----VVAKNANGPSNNMGARIFTFRELATATKNFRQECLIGE   55
AT3G07070_PBL26          ----------KTVNEQ---NKNNDEDKEVTNNIAAQTFSFRELATATKNFRQECLIGE   87
AT2G28590_PBL6           ICGDVS--KEI-VTKKDQLALDAKDTNVEDEVIVKKAQTFTFEELSVSTGNFKSDCFLGE  106
AT3G20530_PBL23          TD----------SSRRRYISE---EIAKLGKGNISAHIFTFRELCVATKNFNPDNQLGE   90
AT5G13160_PBS1           PSGGEKLSSKT-NGGSKR-ELL---LP-RDGLGQIAAHTFAFRELAAATMNFHPDTFLGE   94
AT5G02800_PBL7/CDL1      TS--------E-KSRAKS-SLS---ESKSKGSDHIVAQTFTFSELATATRNFRKECLIGE   81
AT5G18610_PBL27/GCN2     KS-----KSRR-GPEQKK-ELT---APKEGPTAHIAAQTFTFRELAAATKNFRPECLLGE   91
AT1G72540_PBL33          VY--------MSDFSNST----ISLNDFS-NSFFINIHIFTYEELKTITQGFSKYNFLGE   92
AT5G56460_PBL16          -----HIKEVQKLPSNPK-----EVEDLRRDSAANPLIAFTYEELKNITSNFRQDRVLGG   84
AT1G61590_PBL15/SGN1     -----SFAD-LSRSSSAR-----INEDLAQT-LGADLVDFQMCELKMITQSFSGNYLLGE  107
AT2G07180_PBL17          VS-GSGSGG-GGLPLAPK-----NIKDLQSNPGYENVDIFTYEEMKIATKQFRPDYILGE   98
AT2G26290_PBL12/ARSK1    -----SLSD-ISDPSSPM----SVMDDLSHSFTSQKLRLFTLSELRVITHNFSRSNMLGE   96
AT5G01020_PBL8           -----SVSD-LSDPSTPR-----FRDDSRTPISYAQVIPFTLFELETITKSFRPDYILGE   77
AT5G35580_PBL13          -----SILD-ISNPSSTT-----LSEDLSISLAGSDLHVFTQAELRVITQSFSSSNFLGE   84
AT2G05940_PBL14/RIPK     -----SILD-MSNPSSNT-----LSEDLSISLAGSDLHVFTLAELKVITQSFSSTNFLGE   95
AT4G35600_PBL30/CX32     TT-NSS---VGQQSQFSD-ISTGIISDSGKLLESPNLKVYNFLDLKTATKNFKPDSMLGQ   95
AT1G76360_PBL31          ---------PPSKPVEKL-GLGRKAVPPSGKIVTPNLKMFTLVELKTATKNFRPESVIGE  171
AT2G17220_PBL32/KIN3     ---GSN---ISSNSGFSV-ASGEDAYPDGQILPIPNLRIFSLAELRASTRNFRSENVLGE   95
AT3G28690_PBL36          --------APTKDTGCAE-SGSSTPLMSGELKYSSKLRIFMFNDLKLATRNFRPESLLGE  134
AT3G01300_PBL35          --------SSTTTTSNAE-SSLSTPIISEELNIYSHLKKFSFIDLKLATRNFRPESLLGE  144
AT5G15080_PBL34          --------SSTTTTSNAE-SSSSTPVISEELNISSHLRKFTFNDLKLSTRNFRPESLLGE  150
AT2G39660_BIK1           ---------SLSSRKSSS-TVAAAQKTEGEILSSTPVKSFTFNELKLATRNFRPDSVIGE   75
AT3G55450_PBL1           ---------HLSSCKS-S-SSATAHKTEGEILSSTTVKSFSFNELKLATRNFRSDSVVGE  106
AT5G02290_PBL11/NAK      ---------DGSKGSSTA-SFSYMPRTEGEILQNANLKNFSLSELKSATRNFRPDSVVGE   76
AT1G07570_PBL9/APK1A     ---------LGSK-ASSV-SVRPSPRTEGEILQSPNLKSFSFAELKSATRNFRPDSVLGE   87
AT2G28930_PBL10/PK1B     ---------LGSK-SSSV-SIRTNPRTEGEILQSPNLKSFTFAELKAATRNFRPDSVLGE   88
AT1G74490_PBL29          SY-PWSLKPLITRKCEAI-SALPPPHKEGDIMHSQYLKSFTLDELKNATGNFCPESLIGE   99
AT2G02800_PBL3/APK2B     SI-NSY---SS------V-ESLPTPRTEGEILSSPNLKAFTFNELKNATRNFRPDSLLGE   91
AT1G14370_PBL2/APK2A     ST-TSY---STD---SSF-GPLPTLRTEGEILSSPNLKAFTFNELKNATKNFRQDNLLGE   94
AT1G26970_PBL4           TI-QSS---SYNDD-TSV-ASLQTPRSEGELLASPTLKAFTFNELKTATRNFRPDSVIGE   91
AT1G69790_PBL18          TI-PSY---SNNSFTTSS-WSNLTPRSEGELLPSPTLKAFTFNELKTATRNFKPNSMIGE   92
                                                                  :   ::   *  *     :*
```

Extended Data Fig. 4 | L135F is conserved among the PBL clade. Protein alignment of the PBL family. Magenta square: RLCK-VII-5 clade; cyan square: RLCK-VII-8 clade; yellow square: the highly conserved L residue.

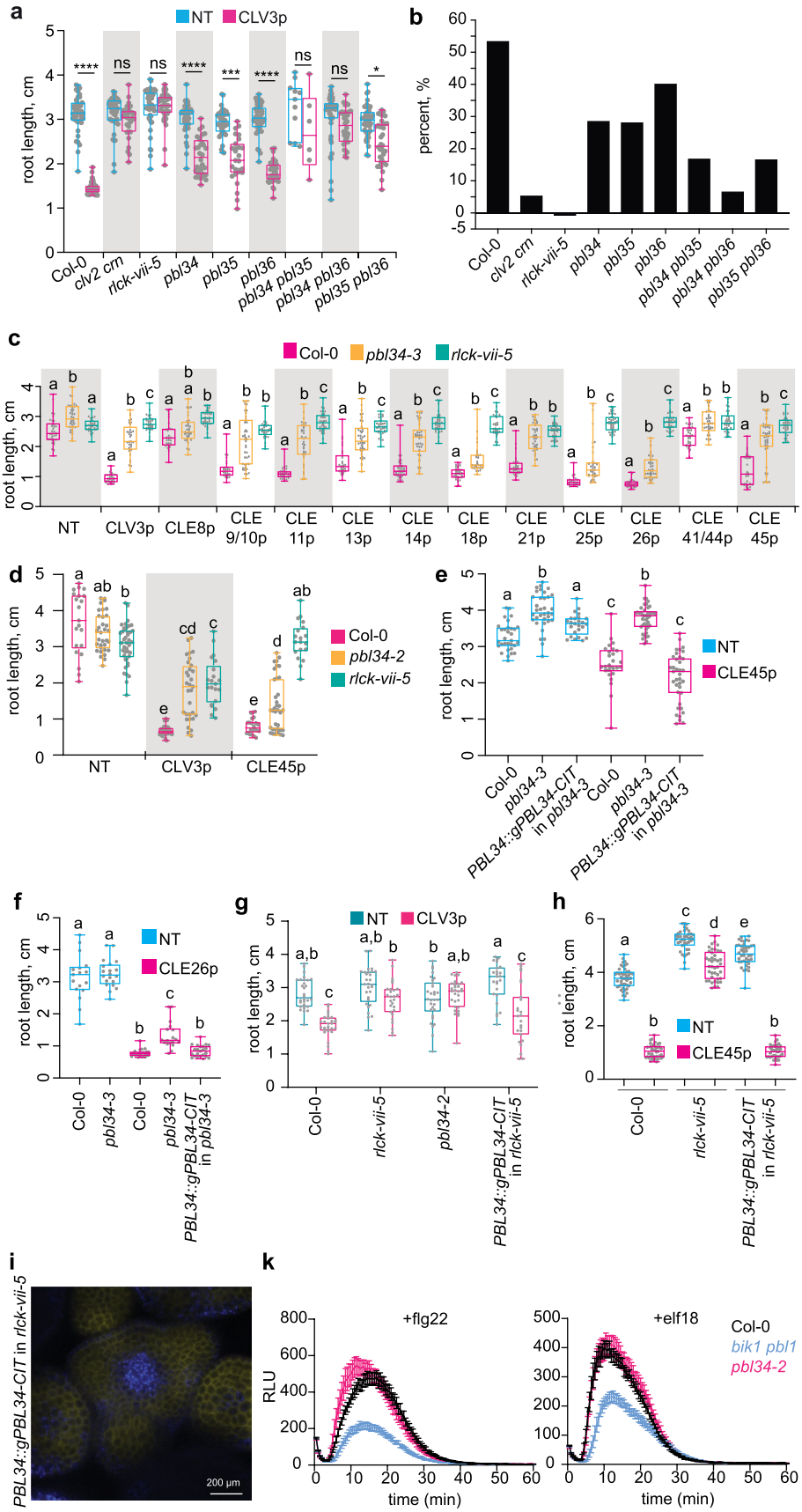

Extended Data Fig. 5 | See next page for caption.

Extended Data Fig. 5 | RLCK-VII-5 clade kinases are specifically required for CLEp perception. (a-c) RLCK-VII-5 members are semi-redundant in the CLEp signalling. (a) Root length of 8-day-old seedlings grown on media with or without 100 nM CLV3p. NT: not treated. Kruskal Wallis non-parametric ANOVA test, **** indicates p value <0.0001, *** indicates p value <0.001, * indicates p value <0.001, ns: not significant, n = 30 independent biological replicates. (b) Corresponding growth ratio inhibition observed in (a) calculated as following: $\left(\frac{root\ length_{NT} - root\ length_{CLV3}}{root\ length_{NT}}\right) x100$. All of the *rlck-vii-5* mutant combinations were less sensitive to CLV3p than the Col-0 background. (**c**) 7-day-old seedlings grown on media with 100 nM of indicated CLE peptides. NT: not treated. Letters indicate significant differences within the treatments (ANOVA followed by Tukey test, two-sided). n = 26–46 independent biological replicates. **(d)** *rlck-vii-5* is less sensitive to CLV3p and CLE45p treatments than the dominant negative *pbl34-2* mutant. 7-day-old seedlings grown on media complemented with 100 nM of indicated peptides. NT: not treated. n = 19–45 independent biological replicates. **(e**,**f)** Complementation of *pbl34-3* mutants expressing *PBL34::gPBL34-CIT* construct. 7-day-old seedlings grown on media complemented with 50 nM CLEp. NT: not treated. Letters indicate significant differences within the treatments (ANOVA followed by Tukey test, two-sided). (e) Complementation assay on CLE45p media, n = 37-58 independent biological replicates. (f) Complementation assay on CLE26p media. n = 17–28 independent biological replicates. **(g**,**h)** Complementation of *rlck-vii-5* mutants expressing *PBL34::gPBL34-CIT* construct. (g) Eight-day-old seedlings grown on media supplemented with 100 nM CLV3p (g; n = 25-31 independent biological replicates) or (h) seven-day-old seedlings grown on media supplemented with 50 nM CLE45p (h; n = 22-47 independent biological replicates). NT: not treated. Letters indicate significant differences within the treatments (ANOVA followed by Tukey test, two-sided). **(i)** Expression of *PBL34::gPBL34-CIT* in the shoot apical meristem. Yellow, PBL34-CIT; blue, chlorophyll. Image represents cross section through L4 of SAM capturing the organizing centre. Low levels of expression were detected in all cell layers and zones of the SAM and developing floral primordia and meristems. **(k)** ROS production in response to 100 nM flg22 or elf18. Curves show mean values ±s.e., n = 12 independent leaf discs. All box plots show 25th to 75th percentile range with a line at the median and whiskers from minimum to maximum values. ROS assays were performed three times with similar results.

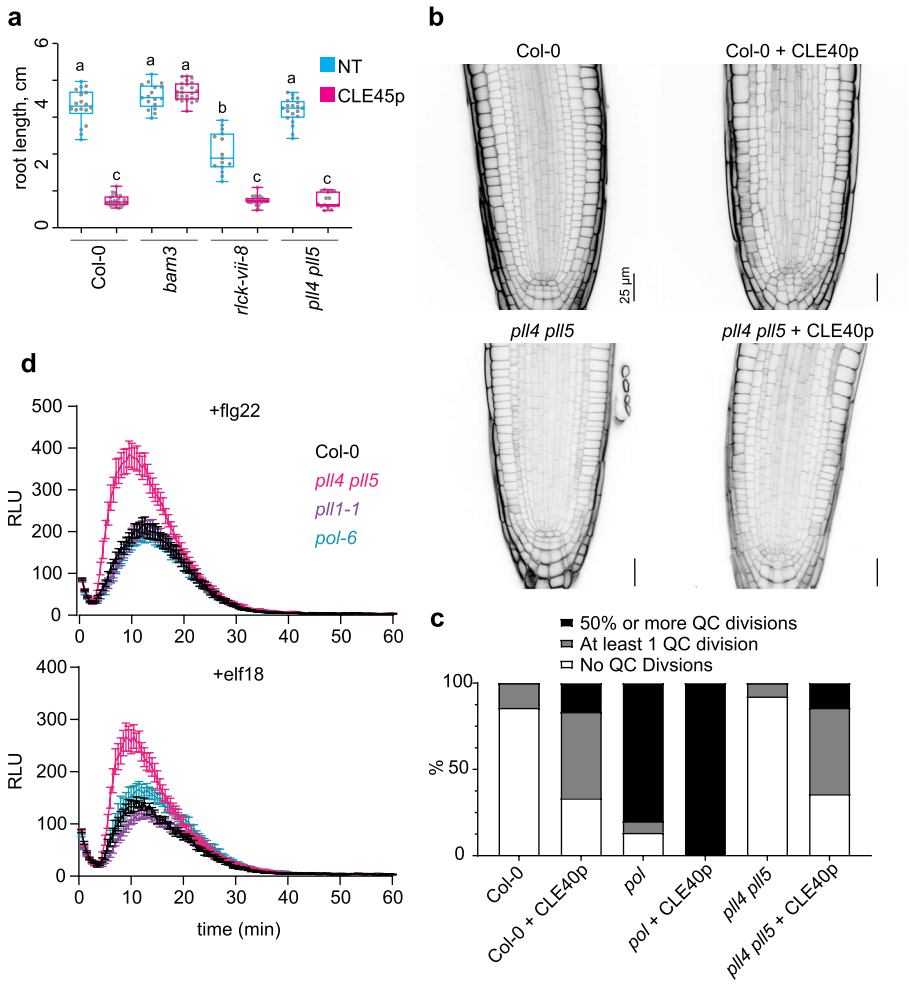

Extended Data Fig. 6 | Pathway-specific roles of PLL family members. (a) Root length of 7-day-old seedlings in response to 15 nM CLE45p. NT = not treated (n = 15–32 independent biological replicates). Different letters indicate statistically significant differences ($p < 0.01$, ANOVA followed by Tukey test, two-sided). Box plots show 25th to 75th percentile range with a line at the median and whiskers from minimum to maximum values. **(b)** QC divisions in response to 100 nM CLE40p. **(c)** Quantification of response shown in (b); n = 10-18 independent biological replicates. **(d)** PAMP-induced ROS in *pll* mutants. Curves show mean values ±s.e., n = 12 independent leaf discs. ROS assays were performed three times with similar results.

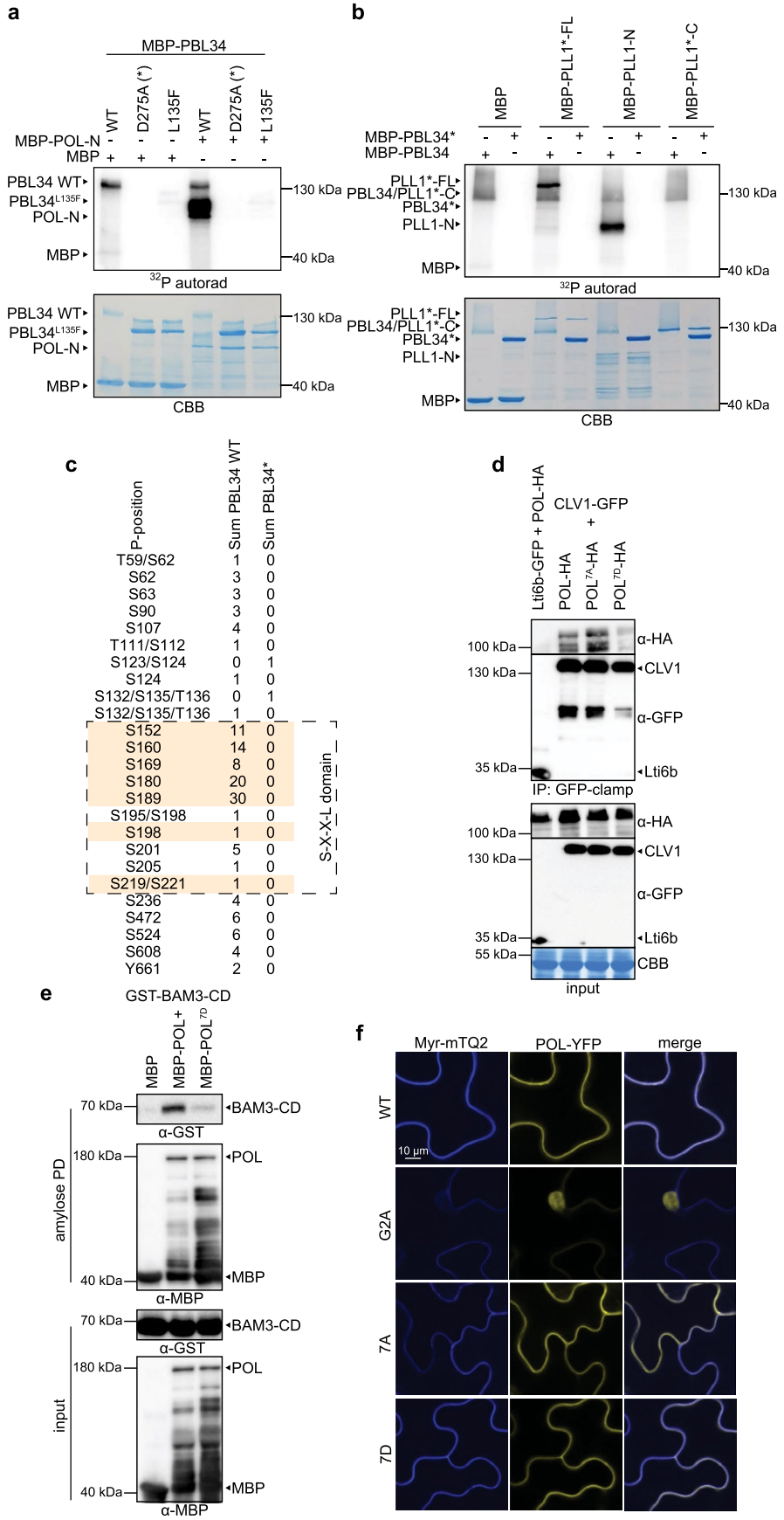

Extended Data Fig. 7 | See next page for caption.

Extended Data Fig. 7 | Conservation of RK-PBL-PLL circuitry in CLEp signalling. (**a**) POL is a substrate of active PBL34. Autoradiogram of *in vitro* kinase assay incubating equal amounts of MBP-tagged POL with MBP-tagged WT PBL34 or mutant forms of PBL34 (PBL34^{D275A} or PBL34^{L135F}). **(b)** PBL34 phosphorylates PLL1 *in vitro*. *In vitro* kinase assay incubating equal amounts of MBP-tagged WT version (PBL34) or inactive (PBL34*) of PBL34 recombinant protein with MBP-tagged N terminus (PLL1-N), catalytically dead full-length (PLL1*-FL), or catalytically dead C-terminus (PLL1*-C). CBB: Coomassie brilliant blue. Kinase assays in (a) and (b) were performed twice with similar results. (**c**) PBL34-dependent MBP-POL phosphosites identified by LC–MS/MS following *in vitro* kinase assays. Numbers indicate sum of total spectra identified across 3 replicates corresponding to phosphorylation at the specified residue(s) in POL. Some spectra were ambiguous for two phosphorylation positions. Sites within the S-X-X-L domain of POL are outlined and spectra corresponding to sites targeted for mutagenesis are highlighted. **(d)** POL phosphorylation status determines its interaction with CLV1 *in planta*. CoIP assay of GFP-tagged CLV1 with HA-tagged WT POL or phosphovariants (POL^{7A} or POL^{7D}). **(e)** POL phosphosites control direct interaction with BAM3 *in vitro*. Amylose pulldown assay using equal amounts of GST-tagged cytosolic domain (CD) of BAM3 with MBP-tagged WT (POL) or phosphomimetic (POL^{7D}) variants of POL. Experiments in (d) and (e) were performed three times with similar results. **(f)** S-X-X-L phosphorylation does not regulate POL-YFP accumulation at the plasma membrane. Confocal images showing POL-YFP (WT or mutant variants; yellow channel) and Myr-mTQ2 (myristoylatable-mTurquoise2, PM marker; blue channel) following co-expression in *N. benthamiana* leaves.

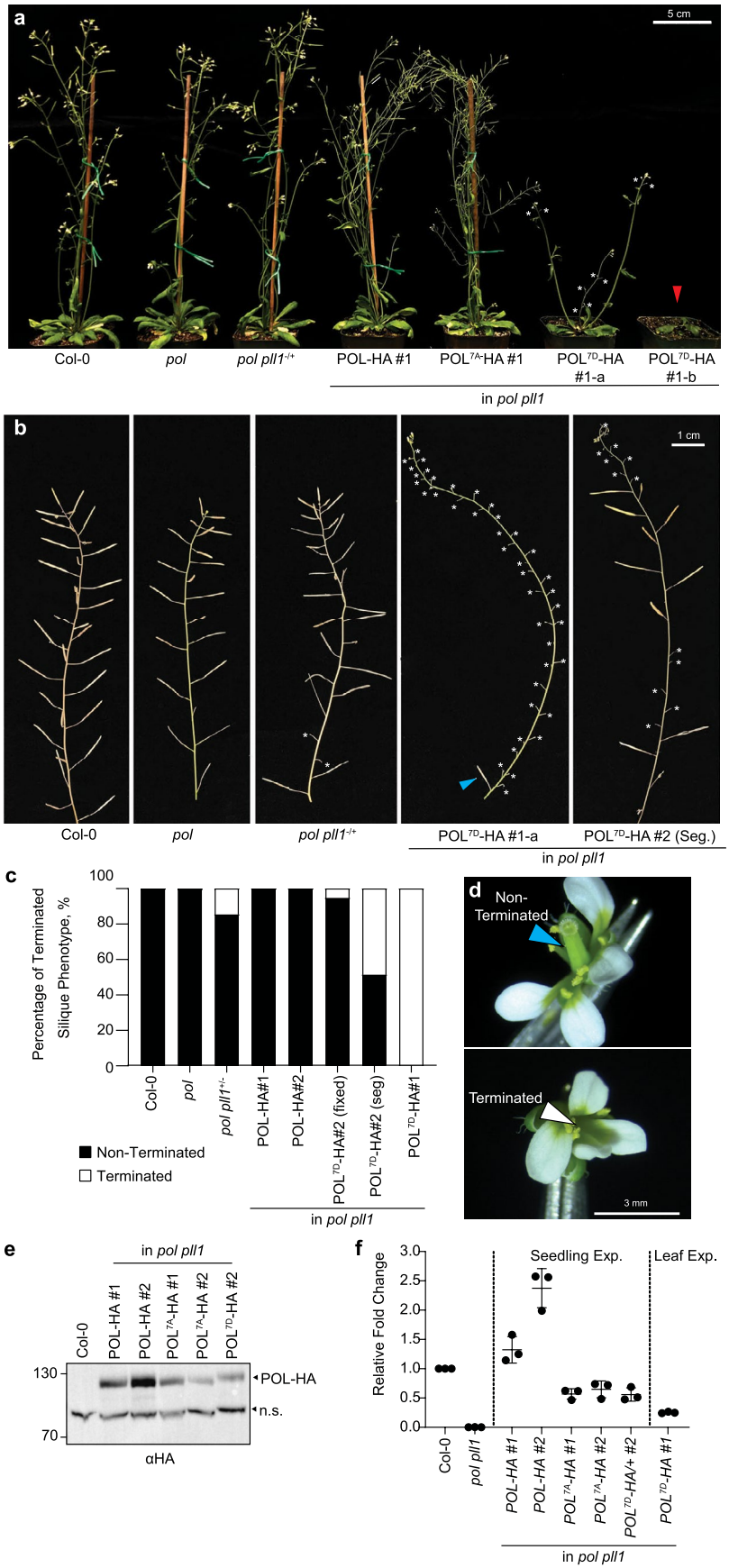

Extended Data Fig. 8 | See next page for caption.

Extended Data Fig. 8 | PBL-phosphorylation sites negatively regulate POL function. (a-c) POL phosphovariants complement *pol pll1* to varying degrees. (a) Representative pictures of 4-week-old plants expressing different phosphovariants of POL-HA protein fusion (WT, POL^{7D} or POL^{7A}) under control of native POL promoter. (b) Representative pictures of 6-week-old stems displaying post-seedling stem cell defect-terminated silique phenotype. white asterisk: terminated silique; cyan arrow head: one successful silique formation for entire line of POL^{7D}-HA #1. (c) Corresponding quantification of the shoot complementation based on terminated silique phenotype. $n \geq 942$ siliques from ≥30 independent biological replicates (plants) per genotype. **(d)** Detailed pictures of terminated flower compared to WT non-terminated one. cyan arrow head: presence of the pistil; white arrow head: absence of pistil. Scale bar: 3 mm. **(e)** Western blot showing expression of POL-HA in *POL::POL-HA* complementation lines. **(f)** Relative fold change ($\Delta\Delta C_T$) expression analysis of *POL* in complementation lines. $n = 3$ independent biological replicates. Error bars indicate ±SD.

nature research

Corresponding author(s): Cyril Zipfel, Christian Hardtke, Zachary Nimchuk

Last updated by author(s): Mar 01, 2022

Reporting Summary

Nature Research wishes to improve the reproducibility of the work that we publish. This form provides structure for consistency and transparency in reporting. For further information on Nature Research policies, see our Editorial Policies and the Editorial Policy Checklist.

Statistics

For all statistical analyses, confirm that the following items are present in the figure legend, table legend, main text, or Methods section.

n/a	Confirmed
☐	☒ The exact sample size (*n*) for each experimental group/condition, given as a discrete number and unit of measurement
☐	☒ A statement on whether measurements were taken from distinct samples or whether the same sample was measured repeatedly
☐	☒ The statistical test(s) used AND whether they are one- or two-sided *Only common tests should be described solely by name; describe more complex techniques in the Methods section.*
☐	☒ A description of all covariates tested
☐	☒ A description of any assumptions or corrections, such as tests of normality and adjustment for multiple comparisons
☐	☒ A full description of the statistical parameters including central tendency (e.g. means) or other basic estimates (e.g. regression coefficient) AND variation (e.g. standard deviation) or associated estimates of uncertainty (e.g. confidence intervals)
☐	☒ For null hypothesis testing, the test statistic (e.g. *F*, *t*, *r*) with confidence intervals, effect sizes, degrees of freedom and *P* value noted *Give P values as exact values whenever suitable.*
☒	☐ For Bayesian analysis, information on the choice of priors and Markov chain Monte Carlo settings
☒	☐ For hierarchical and complex designs, identification of the appropriate level for tests and full reporting of outcomes
☒	☐ Estimates of effect sizes (e.g. Cohen's *d*, Pearson's *r*), indicating how they were calculated

Our web collection on statistics for biologists contains articles on many of the points above.

Software and code

Policy information about availability of computer code

Data collection	Photek charge-coupled device camera and Image32 v5 for ROS measurements; ImageLab 6; Leica SP8, Zeiss 880, and Zeiss 710 for confocal imaging; Epson Perfection V600 Photo and Epson Scan for the scanning of seedlings
Data analysis	GraphPad Prism 8; Microsoft Excel 2016; Image32 v5; ImageLab 6; Inkscape 0.92; Fiji v2.1.0/1.53i and pertinent plugins for image analysis; Rstudio Version 1.0.153; CLUSTALW; MEGA X;

For manuscripts utilizing custom algorithms or software that are central to the research but not yet described in published literature, software must be made available to editors and reviewers. We strongly encourage code deposition in a community repository (e.g. GitHub). See the Nature Research guidelines for submitting code & software for further information.

Data

Policy information about availability of data

All manuscripts must include a data availability statement. This statement should provide the following information, where applicable:

- Accession codes, unique identifiers, or web links for publicly available datasets
- A list of figures that have associated raw data
- A description of any restrictions on data availability

Identifiers for published or publicly available lines are provided in the Methods. The mass spectrometry proteomics data have been deposited to the ProteomeXchange Consortium via the PRIDE partner repository with the dataset identifier PXD031441 and 10.6019/PXD031441. All other relevant data are available from the corresponding authors upon request.

Field-specific reporting

Please select the one below that is the best fit for your research. If you are not sure, read the appropriate sections before making your selection.

☒ Life sciences ☐ Behavioural & social sciences ☐ Ecological, evolutionary & environmental sciences

For a reference copy of the document with all sections, see nature.com/documents/nr-reporting-summary-flat.pdf

Life sciences study design

All studies must disclose on these points even when the disclosure is negative.

Sample size	No sample size calculations were performed before experiments. Sample sizes were chosen empirically based on prior experience to provide statistically robust data (Student's t-test or Fisher's exact test), with n typically 20-30 or higher.
Data exclusions	
Replication	All data were replicable and the number of replicates performed are indicated in the appropriate figure captions or the Methods.
Randomization	Sampling of leaf discs was performed by randomly selecting leaves from individual plants grown in uniform conditions and with different genotypes grown in the same growth chamber. Randomization was not relevant to biochemical assays in this study due to discrete controls.
Blinding	Blinding was not relevant for the biochemical assays in this experiment due to discrete controls. Other assays did not require blinding where data collection was automated.

Reporting for specific materials, systems and methods

We require information from authors about some types of materials, experimental systems and methods used in many studies. Here, indicate whether each material, system or method listed is relevant to your study. If you are not sure if a list item applies to your research, read the appropriate section before selecting a response.

Materials & experimental systems

n/a	Involved in the study
☐	☒ Antibodies
☒	☐ Eukaryotic cell lines
☒	☐ Palaeontology and archaeology
☒	☐ Animals and other organisms
☒	☐ Human research participants
☒	☐ Clinical data
☒	☐ Dual use research of concern

Methods

n/a	Involved in the study
☒	☐ ChIP-seq
☒	☐ Flow cytometry
☒	☐ MRI-based neuroimaging

Antibodies

Antibodies used	For blotting: α-GFP-GFP (Santa Cruz sc-9996, 1:5000 dilution, lot #L0419); α-HA-HRP (Roche 12013819001, 1:3000 dilution, lot #14847700); α-polyhistidine (Sigma H1029, 1:5000 dilution, lot #0000093769); α-MBP (NEB E8032S, 1:5000 dilution, lot# 10081890); α-phosphothreonine (Cell Signaling Technology 9381, 1:2000 dilution, lot #25); α-mouse IgG-HRP (Sigma A0168, 1:10000 dilution, lot #080M4839); α-HA (Roche 11867423001, 1:1000, lot #21319000); α-rat IgG-HRP (Santa Cruz sc-2750, 1:5000 dilution, lot# H0211); α-GST (Upstate 06332, 1:10000 dilution). For immunolocalization: α-GFP (Abcam ab290, 1:600 dilution, lot #GR3196305); α-rabbit Alexa Fluor 546 (Life Technologies A-11010, 1:500 dilution, lot #1600212)
Validation	Validation statements for commercial antibodies are available from the corresponding manufacturers' websites. For α-phosphothreonine, validation against EFR was performed using WT and kinase-dead variants of MBP-EFR-CD protein.

Eukaryotic cell lines

Policy information about cell lines

Cell line source(s)	*State the source of each cell line used.*
Authentication	*Describe the authentication procedures for each cell line used OR declare that none of the cell lines used were authenticated.*
Mycoplasma contamination	*Confirm that all cell lines tested negative for mycoplasma contamination OR describe the results of the testing for mycoplasma contamination OR declare that the cell lines were not tested for mycoplasma contamination.*

Commonly misidentified lines
(See ICLAC register)

Name any commonly misidentified cell lines used in the study and provide a rationale for their use.

Palaeontology and Archaeology

Specimen provenance

Provide provenance information for specimens and describe permits that were obtained for the work (including the name of the issuing authority, the date of issue, and any identifying information).

Specimen deposition

Indicate where the specimens have been deposited to permit free access by other researchers.

Dating methods

If new dates are provided, describe how they were obtained (e.g. collection, storage, sample pretreatment and measurement), where they were obtained (i.e. lab name), the calibration program and the protocol for quality assurance OR state that no new dates are provided.

☐ Tick this box to confirm that the raw and calibrated dates are available in the paper or in Supplementary Information.

Ethics oversight

Identify the organization(s) that approved or provided guidance on the study protocol, OR state that no ethical approval or guidance was required and explain why not.

Note that full information on the approval of the study protocol must also be provided in the manuscript.

Animals and other organisms

Policy information about studies involving animals; ARRIVE guidelines recommended for reporting animal research

Laboratory animals

For laboratory animals, report species, strain, sex and age OR state that the study did not involve laboratory animals.

Wild animals

Provide details on animals observed in or captured in the field; report species, sex and age where possible. Describe how animals were caught and transported and what happened to captive animals after the study (if killed, explain why and describe method; if released, say where and when) OR state that the study did not involve wild animals.

Field-collected samples

For laboratory work with field-collected samples, describe all relevant parameters such as housing, maintenance, temperature, photoperiod and end-of-experiment protocol OR state that the study did not involve samples collected from the field.

Ethics oversight

Identify the organization(s) that approved or provided guidance on the study protocol, OR state that no ethical approval or guidance was required and explain why not.

Note that full information on the approval of the study protocol must also be provided in the manuscript.

Human research participants

Policy information about studies involving human research participants

Population characteristics

Describe the covariate-relevant population characteristics of the human research participants (e.g. age, gender, genotypic information, past and current diagnosis and treatment categories). If you filled out the behavioural & social sciences study design questions and have nothing to add here, write "See above."

Recruitment

Describe how participants were recruited. Outline any potential self-selection bias or other biases that may be present and how these are likely to impact results.

Ethics oversight

Identify the organization(s) that approved the study protocol.

Note that full information on the approval of the study protocol must also be provided in the manuscript.

Clinical data

Policy information about clinical studies

All manuscripts should comply with the ICMJE guidelines for publication of clinical research and a completed CONSORT checklist must be included with all submissions.

Clinical trial registration

Provide the trial registration number from ClinicalTrials.gov or an equivalent agency.

Study protocol

Note where the full trial protocol can be accessed OR if not available, explain why.

Data collection

Describe the settings and locales of data collection, noting the time periods of recruitment and data collection.

Outcomes

Describe how you pre-defined primary and secondary outcome measures and how you assessed these measures.

Dual use research of concern

Policy information about dual use research of concern

Hazards

Could the accidental, deliberate or reckless misuse of agents or technologies generated in the work, or the application of information presented in the manuscript, pose a threat to:

No	Yes	
☐	☐	Public health
☐	☐	National security
☐	☐	Crops and/or livestock
☐	☐	Ecosystems
☐	☐	Any other significant area

Experiments of concern

Does the work involve any of these experiments of concern:

No	Yes	
☐	☐	Demonstrate how to render a vaccine ineffective
☐	☐	Confer resistance to therapeutically useful antibiotics or antiviral agents
☐	☐	Enhance the virulence of a pathogen or render a nonpathogen virulent
☐	☐	Increase transmissibility of a pathogen
☐	☐	Alter the host range of a pathogen
☐	☐	Enable evasion of diagnostic/detection modalities
☐	☐	Enable the weaponization of a biological agent or toxin
☐	☐	Any other potentially harmful combination of experiments and agents

ChIP-seq

Data deposition

☐ Confirm that both raw and final processed data have been deposited in a public database such as GEO.

☐ Confirm that you have deposited or provided access to graph files (e.g. BED files) for the called peaks.

Data access links *May remain private before publication.*	*For "Initial submission" or "Revised version" documents, provide reviewer access links. For your "Final submission" document, provide a link to the deposited data.*
Files in database submission	*Provide a list of all files available in the database submission.*
Genome browser session (e.g. UCSC)	*Provide a link to an anonymized genome browser session for "Initial submission" and "Revised version" documents only, to enable peer review. Write "no longer applicable" for "Final submission" documents.*

Methodology

Replicates	*Describe the experimental replicates, specifying number, type and replicate agreement.*
Sequencing depth	*Describe the sequencing depth for each experiment, providing the total number of reads, uniquely mapped reads, length of reads and whether they were paired- or single-end.*
Antibodies	*Describe the antibodies used for the ChIP-seq experiments; as applicable, provide supplier name, catalog number, clone name, and lot number.*
Peak calling parameters	*Specify the command line program and parameters used for read mapping and peak calling, including the ChIP, control and index files used.*
Data quality	*Describe the methods used to ensure data quality in full detail, including how many peaks are at FDR 5% and above 5-fold enrichment.*
Software	*Describe the software used to collect and analyze the ChIP-seq data. For custom code that has been deposited into a community repository, provide accession details.*

Flow Cytometry

Plots

Confirm that:

☐ The axis labels state the marker and fluorochrome used (e.g. CD4-FITC).

☐ The axis scales are clearly visible. Include numbers along axes only for bottom left plot of group (a 'group' is an analysis of identical markers).

☐ All plots are contour plots with outliers or pseudocolor plots.

☐ A numerical value for number of cells or percentage (with statistics) is provided.

Methodology

Sample preparation	*Describe the sample preparation, detailing the biological source of the cells and any tissue processing steps used.*
Instrument	*Identify the instrument used for data collection, specifying make and model number.*
Software	*Describe the software used to collect and analyze the flow cytometry data. For custom code that has been deposited into a community repository, provide accession details.*
Cell population abundance	*Describe the abundance of the relevant cell populations within post-sort fractions, providing details on the purity of the samples and how it was determined.*
Gating strategy	*Describe the gating strategy used for all relevant experiments, specifying the preliminary FSC/SSC gates of the starting cell population, indicating where boundaries between "positive" and "negative" staining cell populations are defined.*

☐ Tick this box to confirm that a figure exemplifying the gating strategy is provided in the Supplementary Information.

Magnetic resonance imaging

Experimental design

Design type	*Indicate task or resting state; event-related or block design.*
Design specifications	*Specify the number of blocks, trials or experimental units per session and/or subject, and specify the length of each trial or block (if trials are blocked) and interval between trials.*
Behavioral performance measures	*State number and/or type of variables recorded (e.g. correct button press, response time) and what statistics were used to establish that the subjects were performing the task as expected (e.g. mean, range, and/or standard deviation across subjects).*

Acquisition

Imaging type(s)	*Specify: functional, structural, diffusion, perfusion.*
Field strength	*Specify in Tesla*
Sequence & imaging parameters	*Specify the pulse sequence type (gradient echo, spin echo, etc.), imaging type (EPI, spiral, etc.), field of view, matrix size, slice thickness, orientation and TE/TR/flip angle.*
Area of acquisition	*State whether a whole brain scan was used OR define the area of acquisition, describing how the region was determined.*

Diffusion MRI ☐ Used ☐ Not used

Preprocessing

Preprocessing software	*Provide detail on software version and revision number and on specific parameters (model/functions, brain extraction, segmentation, smoothing kernel size, etc.).*
Normalization	*If data were normalized/standardized, describe the approach(es): specify linear or non-linear and define image types used for transformation OR indicate that data were not normalized and explain rationale for lack of normalization.*
Normalization template	*Describe the template used for normalization/transformation, specifying subject space or group standardized space (e.g. original Talairach, MNI305, ICBM152) OR indicate that the data were not normalized.*
Noise and artifact removal	*Describe your procedure(s) for artifact and structured noise removal, specifying motion parameters, tissue signals and physiological signals (heart rate, respiration).*

Volume censoring

Define your software and/or method and criteria for volume censoring, and state the extent of such censoring.

Statistical modeling & inference

Model type and settings

Specify type (mass univariate, multivariate, RSA, predictive, etc.) and describe essential details of the model at the first and second levels (e.g. fixed, random or mixed effects; drift or auto-correlation).

Effect(s) tested

Define precise effect in terms of the task or stimulus conditions instead of psychological concepts and indicate whether ANOVA or factorial designs were used.

Specify type of analysis: ☐ Whole brain ☐ ROI-based ☐ Both

Statistic type for inference
(See Eklund et al. 2016)

Specify voxel-wise or cluster-wise and report all relevant parameters for cluster-wise methods.

Correction

Describe the type of correction and how it is obtained for multiple comparisons (e.g. FWE, FDR, permutation or Monte Carlo).

Models & analysis

n/a	Involved in the study
☐	☐ Functional and/or effective connectivity
☐	☐ Graph analysis
☐	☐ Multivariate modeling or predictive analysis

Functional and/or effective connectivity

Report the measures of dependence used and the model details (e.g. Pearson correlation, partial correlation, mutual information).

Graph analysis

Report the dependent variable and connectivity measure, specifying weighted graph or binarized graph, subject- or group-level, and the global and/or node summaries used (e.g. clustering coefficient, efficiency, etc.).

Multivariate modeling and predictive analysis

Specify independent variables, features extraction and dimension reduction, model, training and evaluation metrics.